

# **A Review of Aeronautical Fatigue Investigations in Sweden During the Period April 2011 to March 2013**



**Edited by HANS ANSELL  
Saab AB  
Sweden**

**ICAF Doc. No. 2430  
Saab Doc. No. LN-009254**



**swerea | SICOMP**

Presented at the 33<sup>th</sup> Conference of the International Committee on Aeronautical Fatigue (ICAF), Jerusalem, Israel, 3-4 June 2013.

## CONTENTS

3.1	INTRODUCTION .....	3
3.2	INVESTIGATIONS ON OPERATIONAL EVENTS.....	4
3.2.1	Saab 340 Windshield side post cracking.....	4
3.2.2	Saab 340 Aileron cracks.....	6
3.3	STRUCTURAL EVALUATION .....	10
3.3.1	The Saab 2000 Full Scale Fatigue Test and Damage tolerance Test - General .....	10
3.3.2	The Saab 2000 Full Scale Fatigue Test of Wing and fuselage .....	10
3.3.3	JAS39 Gripen A/B/C/D Fatigue Testing.....	19
3.3.4	JAS39 Gripen C/D Static strength test of pylons attachments in wing carrying heavy stores .....	19
3.3.5	JAS39 Gripen E test verification programmes for static, damage tolerance and fatigue life .....	20
3.3.6	Damage Tolerance Test and Analysis of Wing Tip Pylons for the Gripen Aircraft.....	21
3.3.7	Fatigue and damage tolerance aspects of hybrid metal-composite wing structures.....	22
3.4	FATIGUE CRACK INITIATION AND PROPAGATION.....	32
3.4.1	A parametric fatigue life prediction method for generic aircraft fitting.....	32
3.4.2	Modelling of high temperature fatigue crack growth in Inconel 718 under hold time conditions.....	34
3.4.3	Topology optimization with respect to stress and fatigue .....	38
3.5	COMPOSITE MATERIALS.....	41
3.5.1	Biaxial testing of composite joint .....	41
3.5.2	Detailed measurements of bearing failure in composite bolted joint.....	43
3.5.3	Enhancing structural efficiency through novel dissimilar material joining techniques .....	46
3.5.4	Cryogenic Hypersonic Advanced Tank Technologies (CHATT).....	47
3.6	NDT TECHNOLOGY .....	48
3.6.1	Detectability of indents after impact in full-scale CFRP wing skins .....	48
3.7	SERVICE LOADS MONITORING.....	50
3.7.1	A flight parametric method for loads and fatigue life monitoring of Gripen C/D aircraft.....	50
	REFERENCES.....	52
	ACKNOWLEDGEMENTS .....	54

### 3.1 INTRODUCTION

In this paper a review is given of the work carried out in Sweden in the area of aeronautical fatigue and structural integrity during the period April 2012 to March 2013. The review includes basic studies and industrial applications of fatigue development in metals and composites, stress analysis and fracture mechanics, studies of crack initiation and propagation and residual strength, service loads monitoring, testing of full-scale structures, non destructive inspection techniques and fatigue life predictions. A reference list of relevant papers issued during the period covered by the review is included.

Contributions to the present review are from the following bodies:

- SAAB AB  
Sections 3.2.1, 3.2.2, 3.3.1, 3.3.2, 3.3.3, 3.3.4, 3.3.5, 3.3.6, 3.3.7, 3.4.1, 3.4.3, 3.5.1, 3.6.1, 3.7.1
- The Swedish Defence Research Agency (FOI)  
Sections 3.3.7, 3.5.1, 3.5.2
- Swerea SICOMP  
Sections 3.3.7, 3.5.3, 3.5.4
- Linköping University (LiU)  
Sections 3.4.2

## 3.2 INVESTIGATIONS ON OPERATIONAL EVENTS

### 3.2.1 Saab 340 Windshield side post cracking

During scheduled maintenance checks of the Saab 340 aircraft it has been noticed that some local cracks have been detected in the forward fuselage windshield side posts as detailed in figure 1. The cracks on aircraft in service are discovered in the present cases between 35000 - 450000 accumulated flights. Inspection methods such as detailed inspections and non destructive testing are called out through out the existing maintenance program in order to discover and verify the presence of possible cracking.

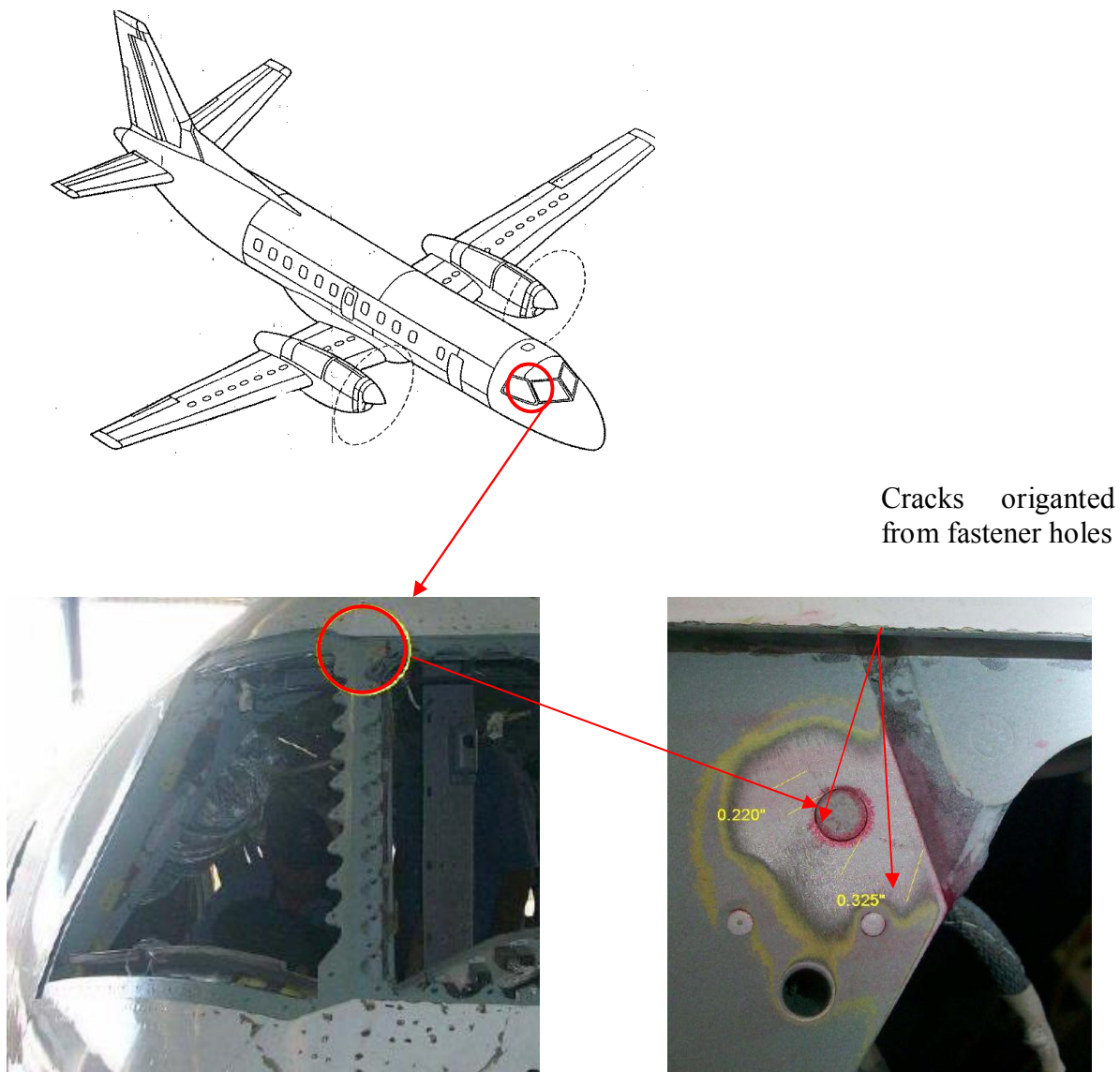


*Figure 3.2.1-1 Location of the area subjected to cracks originated from fastener holes*

A comprehensive investigation has been carried out aiming to augment the reason for the cracking phenomena in window framing. The loading of this corner of the side posts are complex. The stress picture is combination of membrane and bending stresses originating from internal pressure of the forward fuselage.

A number fatigue and damage tolerance tests have been performed on the forward fuselage. Some result from these indicates and support that corners are to some extent sensitive to fatigue loading. However, the test results indicated that cracking may occur after 80000 to 90000 simulated flights.

As the Saab340 aircraft has embodied the fatigue and damage tolerance concept according to regulations FAR/FAR 25.571, long term characteristics test have been carried out verifying the continuing airworthiness. Inspection intervals and residual strength capability considering the presence of possible cracking have accordingly been carried out. On the basis of these results it is deemed the structural integrity of the window framing is not compromised as a result of the cracks.

In order to minimize the impact for the operators in terms of cost and time consuming structural repairs a local reinforcement of the subject has been defined. Analysis using the FEM technology was used to design a preventive reinforcement of the impacted area. Additionally, the authorities does not usually allow continued flight with known cracks even if the don't jeopardize the continuing airworthiness.

There is no regulatory standard for operation with a known crack, except what the authorities accepts on an ad hoc basis in each particular case. The preventive repair consists of the embodiment of local pressure pads to decrease the bending stresses due to internal pressure on the front windows. Figure 2 outlines a portion of Fe model of impacted area used for the design of reinforcing the windshield side post member.

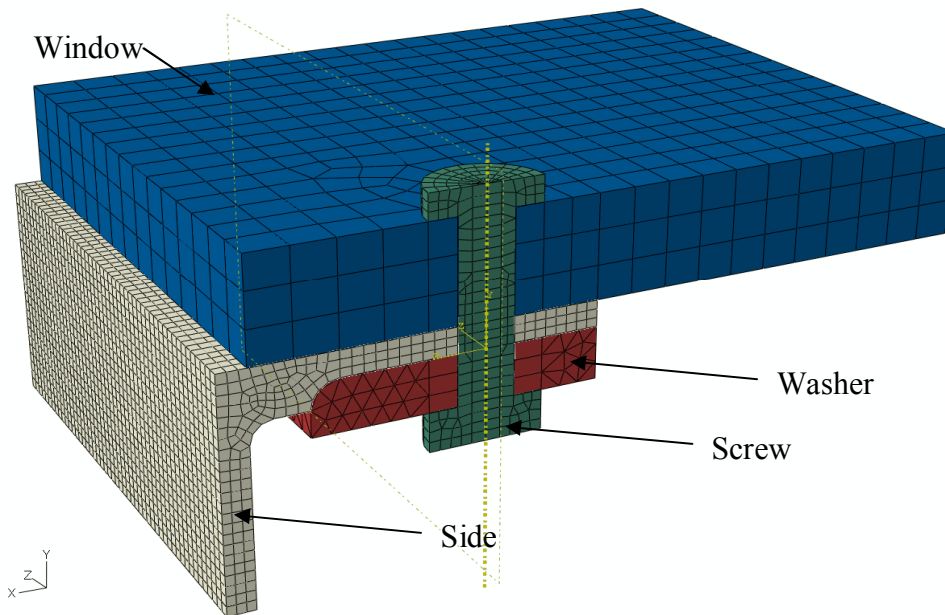


*Figure 3.2.1-2 Fe model of the impacted area*

The engineering assessment concluded that the proposal install pressure pads in the affected will decrease the stress picture due to bending and thereby enhance the long term characteristics of the side post members. Figure 3 details some of the results from the comparative study of the reinforced area.

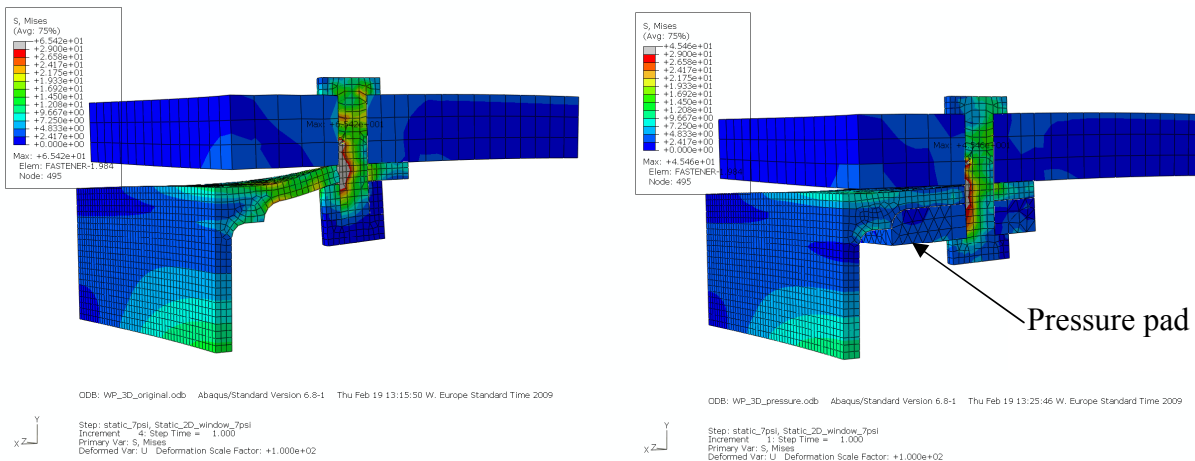


Figure 3.2.1-3 Comparative results of stresses without and with pressure pad

A reduction of the stresses in the subject aluminium members with 25-30 % will enhance the fatigue life of approximately a factor 3.

Summarizing all associated activities from the engineering assessment leads to following conclusions:

- Fatigue cracks in the forward fuselage corner posts may occur on aircraft in service This is based on findings on some findings on aircraft in service and indications from fatigue test of forward fuselages.
- The concerned cracks concerned to the corner posts will still meet the requirement of continuing airworthiness implying that prescribed inspection procedures and residual strength capability has been shown by tests. Limit load tests with significant cracks on the test specimen has been carried out.
- The existing maintenance program has been refined by introducing non destructive testing of both inside and outside area of the side post member.  
The inspection interval has been lowered so that possible cracks can be detected with minor sizes and lengths. Thereby, it is likely to reduce the impact for the airline operators, subsequently minor corrective actions can de defined.
- A Release a non mandatory service bulletin adding pressure pads on the upper attachment of the windshield and side window to the corner post. The subject service bulletin will significantly increase the economic life of the side post members. This will prevent to adopt future cost and time consuming repairs of the side posts members.

### 3.2.2 Saab 340 Aileron cracks

The forward spar of the aileron Saab 340 aircraft has been subjected to cracking. Only a few numbers of ailerons are affected by the cracks in reinforcement angles nested to the forward spar. Figure 3.2.2-1 outlines the location of the crack position.

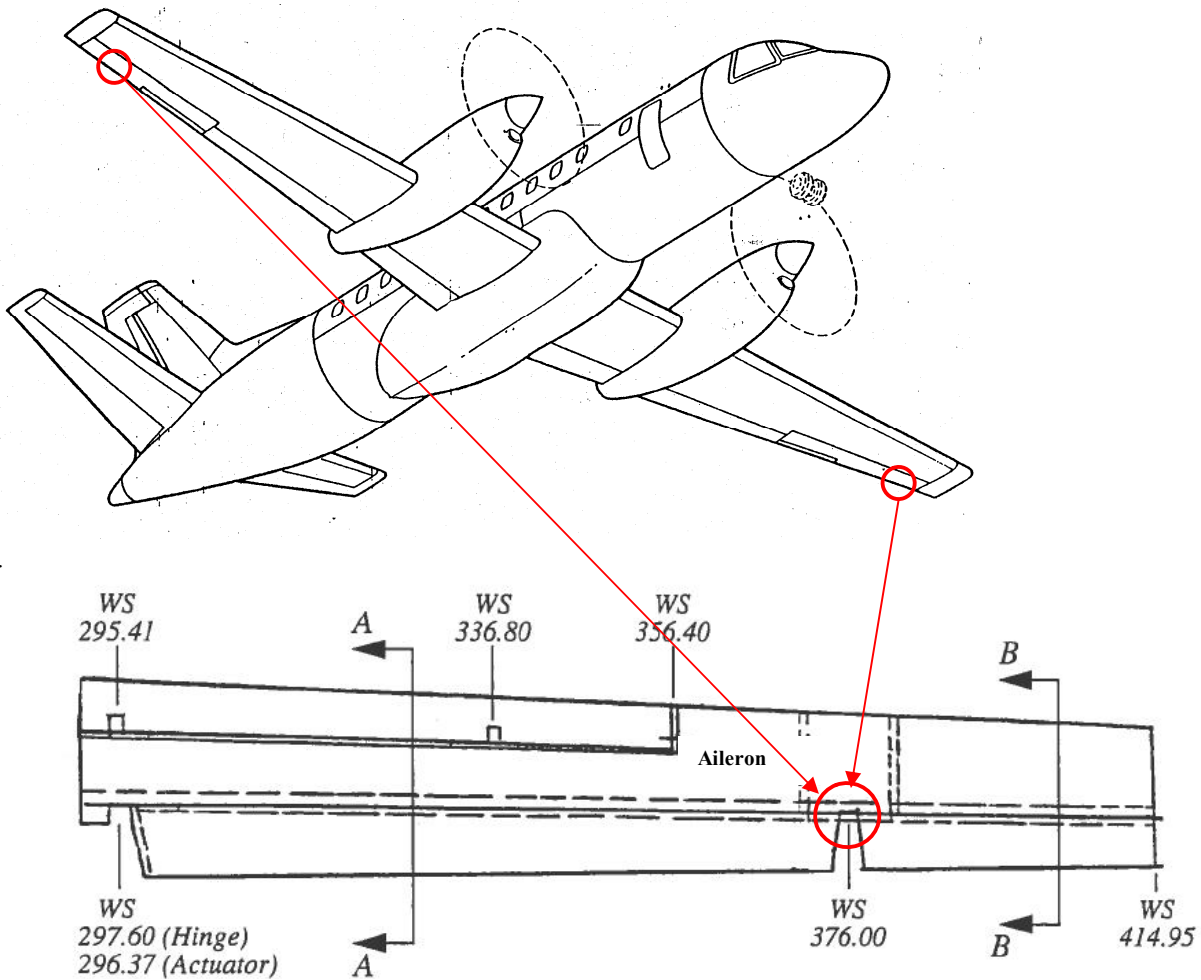


Figure 3.2.2-1 Crack position for cracks in the forward spar of the aileron

The Saab 340 aileron consists of an aluminium alloy front and partial rear spar extending along the trim tab. The inboard cover panels and outboard wedge are made of composite sandwich whilst the leading edge is a fibreglass sandwich construction. The aileron is attached to the wing through two fittings, located at stations WS 297.6 and WS 376.0. At WS 376 there is a local cut out of the spar flange in order accommodate movement of aileron to cut out, local spar reinforcement exists at Station WS 376 in order to compensate for the cut out in the spar. The extent and geometry of the forward spar at WS 376 is detailed in figure 3.2.2-2 below by the green lines.

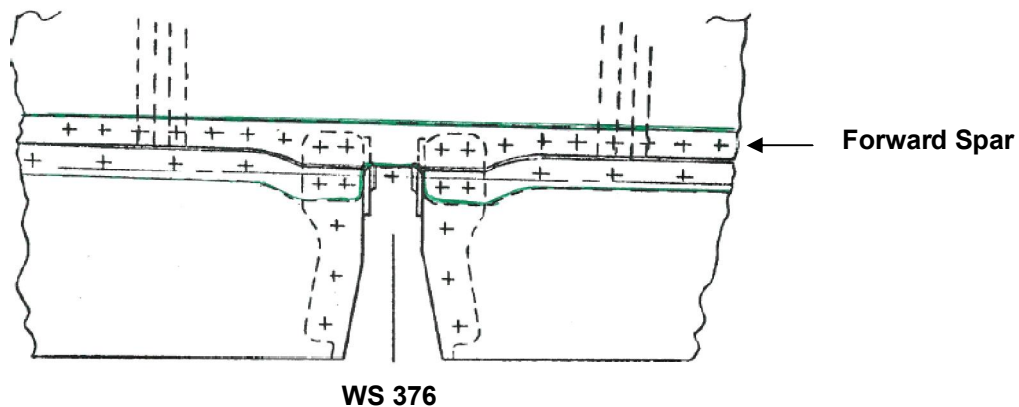


Figure 3.2.2-2 Extent of forward spar and the local cut out of the spar flange at WS 376

The cracking phenomenon is discovered during normal and scheduled inspection according to established maintenance program. Using detailed inspections on the forward spar indicates that cracking are confined to nested angles at station WS376 as depicted in figure 3.2.2-3.

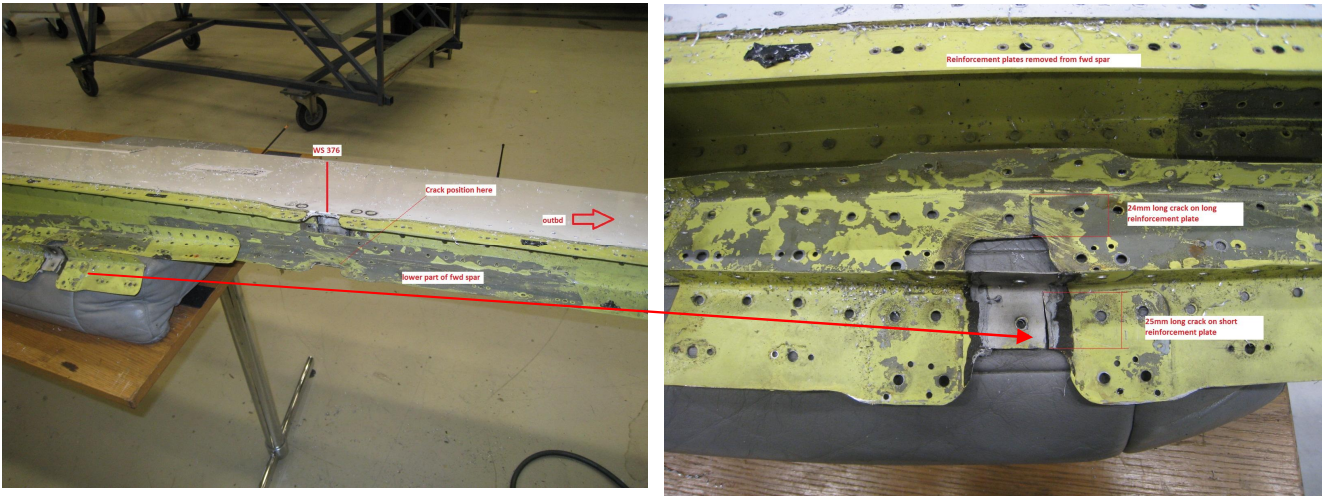


Figure 3.2.2-3 Cracked nested angles on the aileron spar (hinge fitting and leading edge dismantled)

Typical crack lengths are 20-25 mm, initiated from the corner radius of the angles. It is well known that this area is sensitive from fatigue point of view due to a high stressed in combination with an adverse geometry. A classical stress concentration is present as a result of the change in geometry. It should be emphasized that the cracks are confined only to the nested angles however the front spar building up the aileron box is not subjected to any cracking. The overall front spar constitutes of two bonded channels forming the C profile as spar.

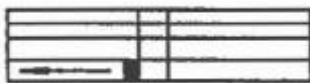
Primary structural elements such as aileron spar have been subjected to damage tolerance analysis and testing in terms of fatigue and damage tolerance testing verifying the overall requirements of fatigue and damage tolerance.

The fatigue test carried out in beginning of the development program resulted in local redesign of the subject area, a pair of nested angles were introduced as a result of some cracking in the latter part of the fatigue testing.

Damage tolerance analysis has been carried out to verify the long term characteristics. A scenario where a crack originates from a fastener hole has been deemed to the most conservative approach. In addition to this, the influence of the change of geometry (associated stress concentration) has also been taken into account. It is also considered crack propagation starts in the one of channels of the overall forward spar.

The following models were used in the crack growth analysis:

Step 1: Crack growth of a primary initial flaw at the edge of the hole in the outer channel. Loads valid for intact structure



Step 2: Continuing crack growth of the secondary crack in the outer channel. Loads valid for intact structure



Step 3 Continuing crack growth of the secondary crack in the inner channel. Loads valid for outer channel broken



Step 4 Continuing crack growth of the secondary crack in the inner channel. Loads valid for outer channel broken



The interpretation of the aforementioned analysis is that structural integrity of the overall spar has been compromised to a such extent that the that limit load capability is only maintained by the nested angles to the spar. The associated crack growth curve is shown in figure 3.2.2-4 outlining that the time to limit load failure is approximately 115000 flights.

Subsequent MSG-3 analyses have concluded in an inspection program in terms of threshold and interval inspection to safely guarantee the continuing airworthiness of the aileron structure. Thereby, the airworthiness requirements addressing are fulfilled.

However, a reassessment of the aileron issue is ongoing aiming to minimize the impact for all airliner operators. Study and actions are to be defined minimizing the economical impact for the operators (avoidance of costly repairs).

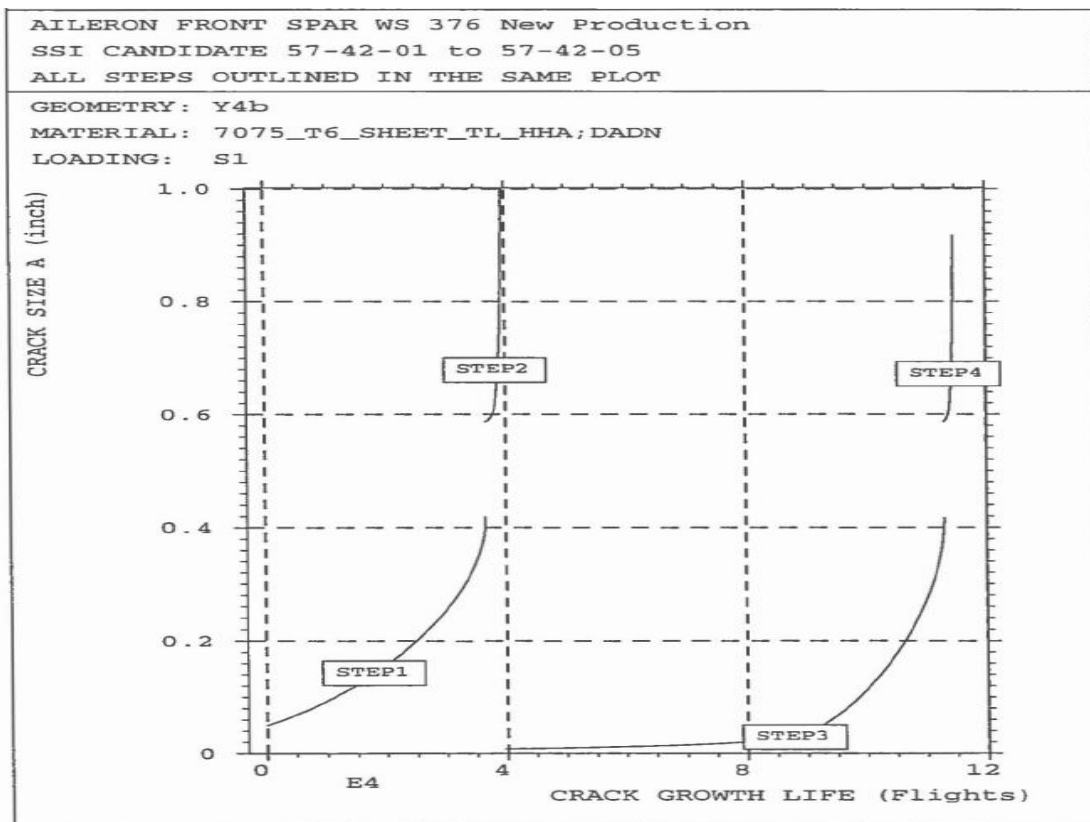


Figure 3.2.2-4 Crack growth curve

### 3.3 STRUCTURAL EVALUATION

#### 3.3.1 The Saab 2000 Full Scale Fatigue Test and Damage tolerance Test - General

The Design Service Goal (DSG) for Saab 2000 is presently 75000 flights or 60000 flight hours whichever occurs first. For the Saab 2000, no complete airframe will be tested due to the commonality with the Saab 340. Consequently, a number of full scale component tests are used to justify the long term characteristics.

#### 3.3.2 The Saab 2000 Full Scale Fatigue Test of Wing and fuselage

The subject test includes the centre and the rear part of the fuselage, the complete wing torque box and the rear part of the engine nacelles.



*Figure 3.3.2-1 Saab 2000 Wing/Fuselage Fatigue and damage tolerance test*

The wing detail design is changed compared to the Saab 340 (machined spars with integral spar caps), and the wing/fuselage interface also. Furthermore the cabin pressurisation spectrum is more severe, more exactly twice as severe as the spectra for the Saab 340 aircraft. The flight and landing loads on the fuselage is also more severe due to the slender fuselage of Saab 2000.

The first part of Wing/Fuselage Fatigue test up to 150000 flights with fatigue loads is finalised. The second part, the damage tolerance testing has been completed in terms of testing up to reach 2\*24000

flights with artificial notches. Twenty six different types of damages have been introduced reflecting the damage tolerance characteristics of various principal structural elements of the Saab 2000 airframe. The third and the last part of testing include testing for verification of the residual strength capability of the airframe. Major artificial cracks representing critical crack length are embodied and subsequently tested for the most critical limit load condition. This part of the test is ongoing.

In conformity with other tests, the wing/fuselage structure has been tested to demonstrate the damage tolerance characteristics in accordance with airworthiness requirements specified in FAA/EASA regulations. This also includes residual strength tests up to limit load condition for selected and critical load cases.

The test sequence used in the damage tolerance phase is the identical to sequence used in the fatigue phase. Thus, this sequence is truncated in terms of reduction of load cycles with small ranges. For damage tolerance testing is also crucial to consider load cycles with small amplitudes or ranges due to the contribution to the total crack propagation. Instead of using a revised test sequence it has been verified that the existing sequence can be adapted with the addition of more test cycles to the previous defined test sequence.

Since a limited no of damages shall represent damage tolerance characteristics of all critical parts, a careful selection has been carried out.

The criteria for selecting which damages to test have been:

- Damages with impact on flight safety
- Damages with short calculated total crack growth life
- Damages in fail safe structure, for which the calculated crack growth life after failure of one load path is short
- Damages for which it is desirable to improve the in-service inspections

The selected damages cover different types of structural parts, such as wing panels, wing spars, fuselage panels, reinforced fuselage cut-outs, wing and fuselage splices. They also cover different types of crack origins, such as for example free edges, open holes and holes with pin load.

Figure 3.3.2-2 on the following pages summarizes the location the artificial cracks introduced on the Saab 2000 airframe.

Figure 3.3.2-3 (damage 19) outlines an artificial crack in the forward lower spar cap including a similar damage to the outer wing skin.

Figure 3.3.2-4 (damage 16) outlines an example of introduced artificial cracks on the lower wing panel, the internal located stringer is also simulated to be broken (through cutting of the entire stringer)

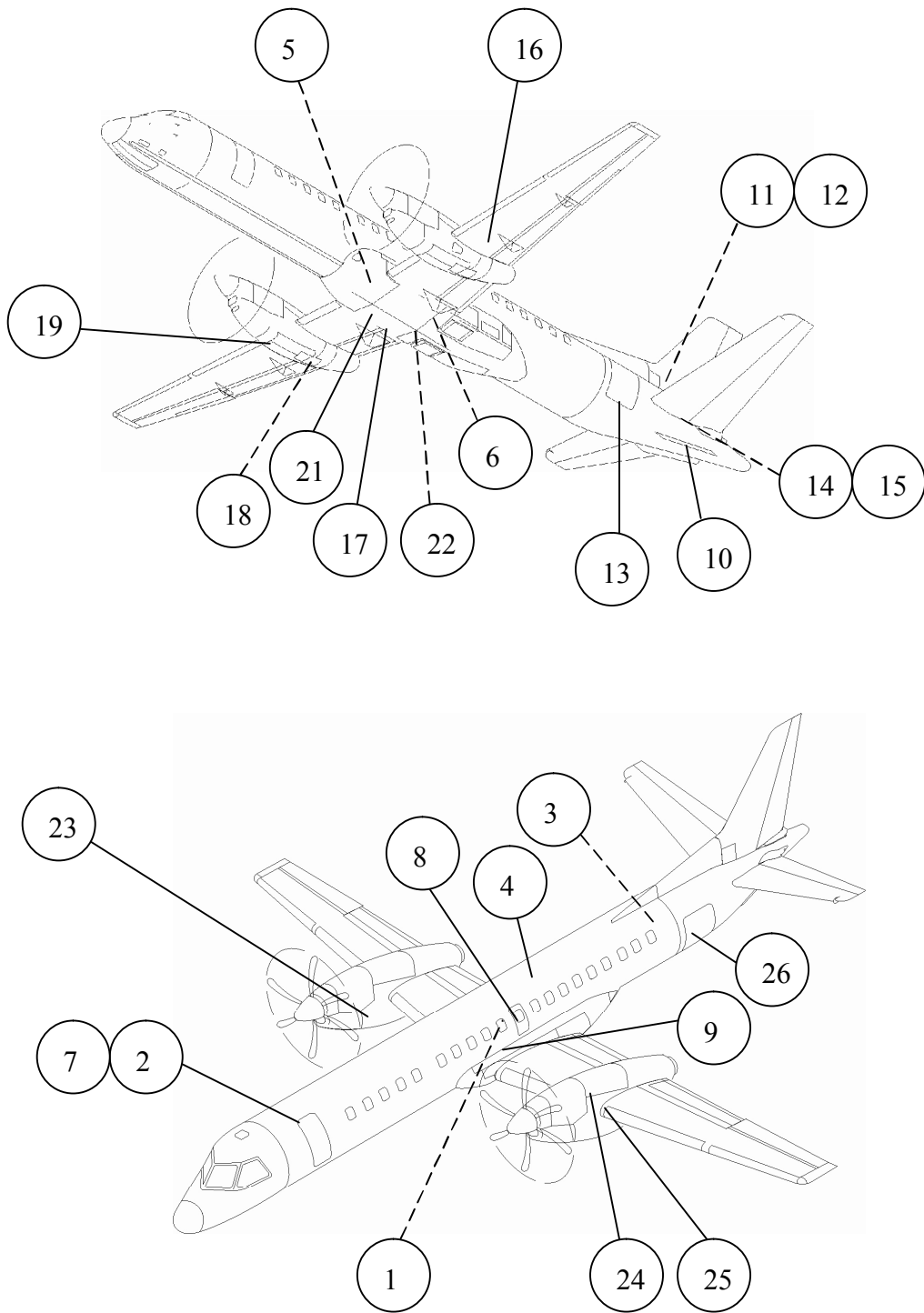
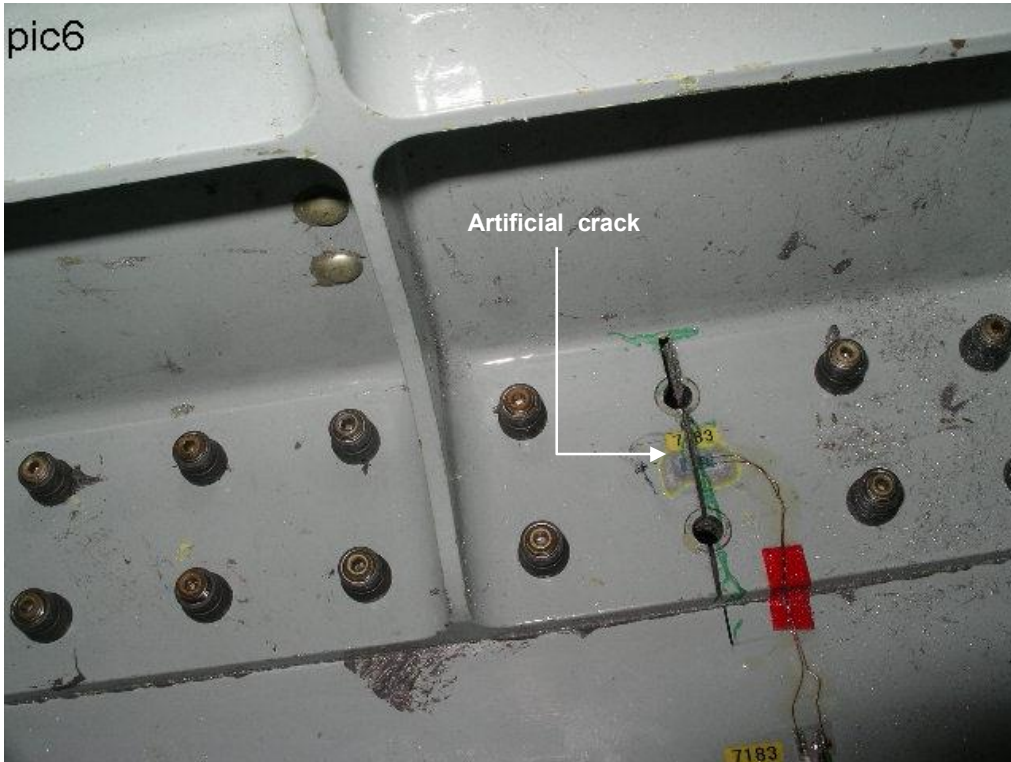
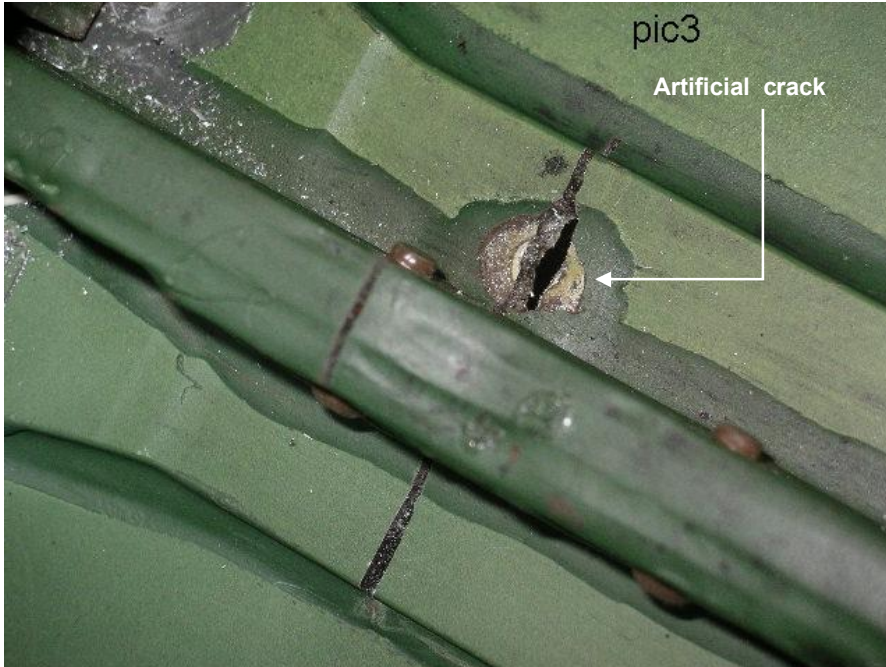


Figure 3.3.2-2 Saab 2000 Overview of artificial cracks in test article



*Figure 3.3.2-3 Saab 2000 Artificial crack in lower forward wing spar cap and in skin*



*Figure 3.3.2-4 Saab 2000 Artificial crack in lower wing skin with a broken stringer*

In general, it is observed that it is hard to have a natural crack growth from an artificial damage. Theoretical crack growth analysis appears to be afflicted with some conservatism. Analytical damage tolerance models are mostly limited in geometry and redistribution of internal loading to adjacent members are not always considered. Consequently, analytical prediction using classical fracture mechanics is deemed to be slightly conservative compared to the results obtained from full scale damage tolerance testing.

However, the artificial crack in the lower wing skin in figure 3.3.2-5 and 3.3.2-6 (damage 16) has been propagated towards the adjacent stringers and crack arrest has been noted at the bonded stringers. The initial crack was 55 mm including a broken stringer, the crack has been propagated 280 mm under 48000 flights of testing. The two-bay crack philosophy has thereby been verified for a predefined inspection interval. By comparison the results from the analysis and the test (see figure 3.3.2-7) it is concluded for this specific artificial damage that the crack growth rate in the theoretical analysis is slightly slower than the observed characteristics from the test article.

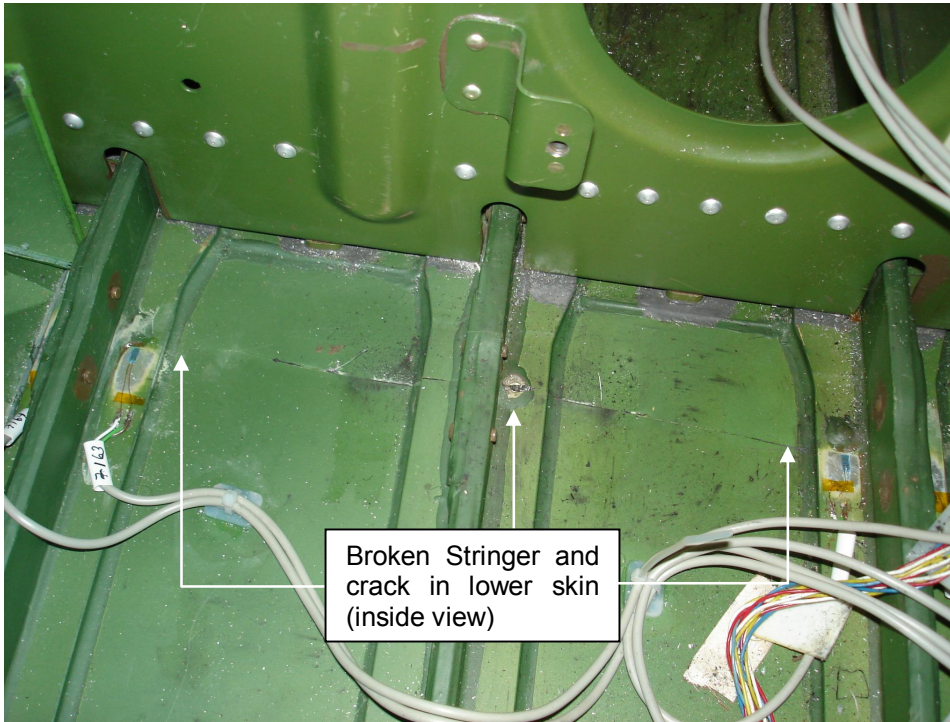


Figure 3.3.2-5 Saab 2000 Artificial crack in lower wing skin and stringer (inside view)

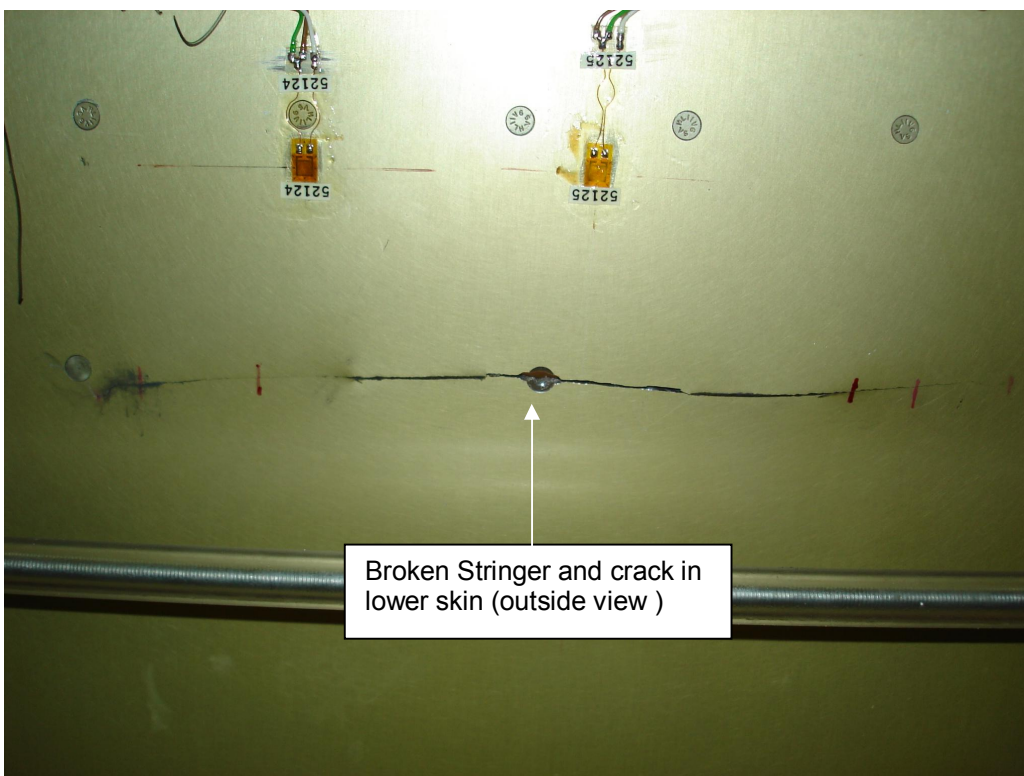


Figure 3.3.2- 6 Saab 2000 Artificial crack in lower wing skin and stringer (outside view)

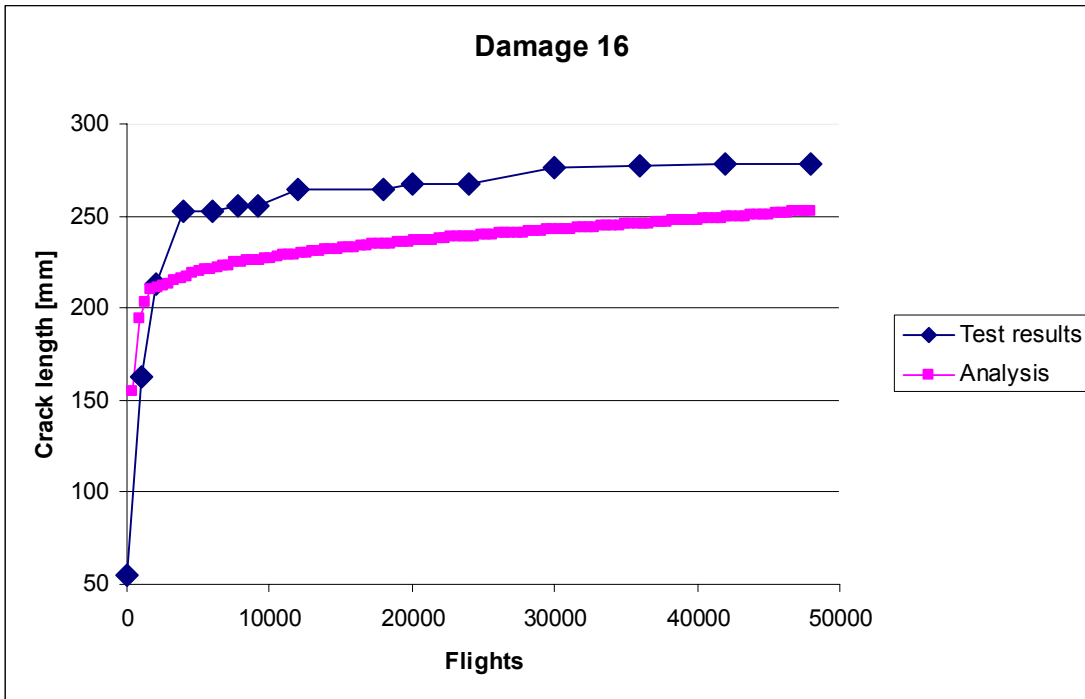


Figure 3.3.2-7 Saab 2000 Artificial crack in lower wing skin and stringer comparison of results

#### Wing/fuselage residual strength testing

The static residual strength test program has been completed implying that the entire airframe was tested covering approximately 20 static limit load cases in order to verify the structure for predetermined critical crack length conditions. Primary structural elements such as circumferential /longitudinal fuselage splices, wing spars and pressure decks were subjected to testing the most critical load case up to limit load level. Figure 3.3.2-8 to 3.3.2-10 outlines some examples of the location and nature of the artificial cracks in pressurized structural members exposed to the residual strength test.

Figure 3.3.2-8 details the artificial crack for the residual test of the mid fuselage pressure deck, the saw cut is approximately 560 mm.

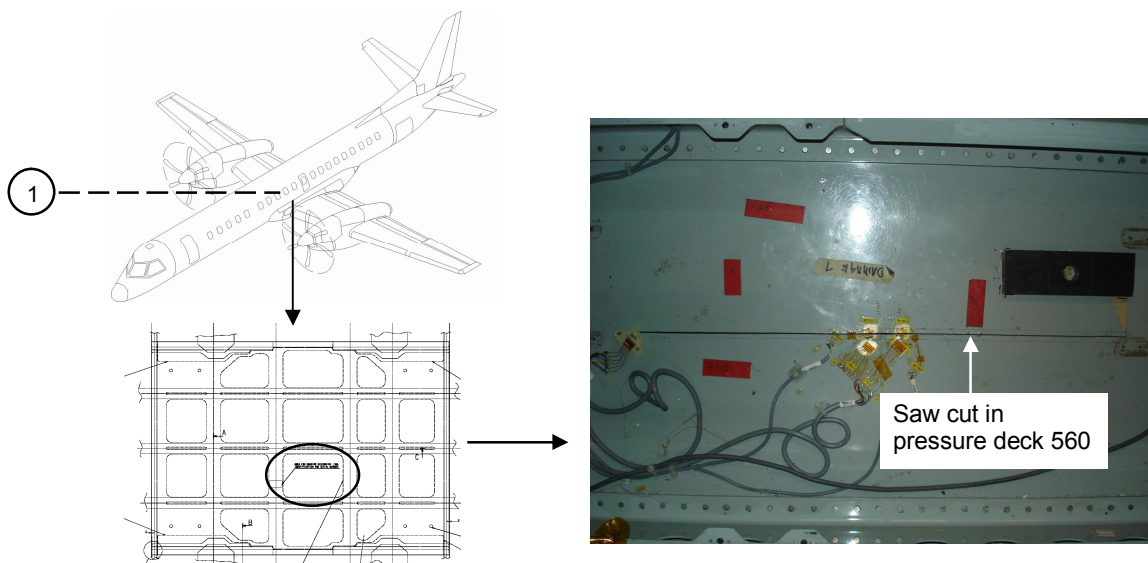


Figure 3.3.2-8 Saab 2000 Artificial crack (saw cut ) for testing of the residual strength capability in the mid pressure deck

The aft pressure bulkhead classified as a principal structural element was exposed to residual strength testing with an associated artificial crack as shown in figure 3.3.2-9. The stiffener including the bulkhead was provided with an artificial crack of 600 mm.

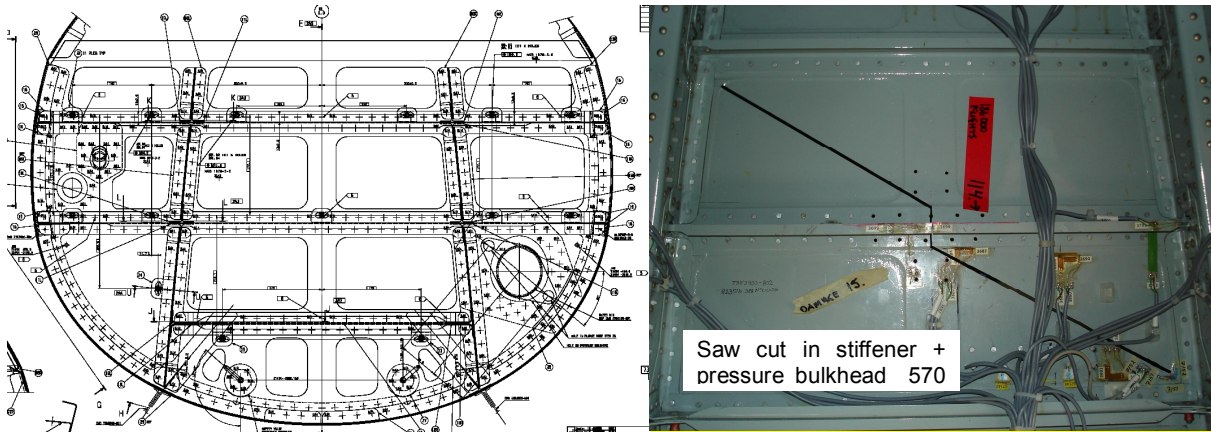


Figure 3.3.2-9. Saab 2000 Artificial crack (saw cut) testing the residual strength capability in the aft pressure bulkhead

The rear wing spar and the adjacent lower skin were tested with respect to residual strength capability where the major portion of the rear wing spar and the lower wing skin has been inflicted with saw cuts. The subject sub-test was made in order to verify the wing structure can withstand all limit load condition considering a major damage to the primary structural elements.

Figure 3.3.2-10 provides the location for the saw cut for the testing. The saw cut in lower skin was approximately 175 mm respectively 70 mm as depicted in the figure.

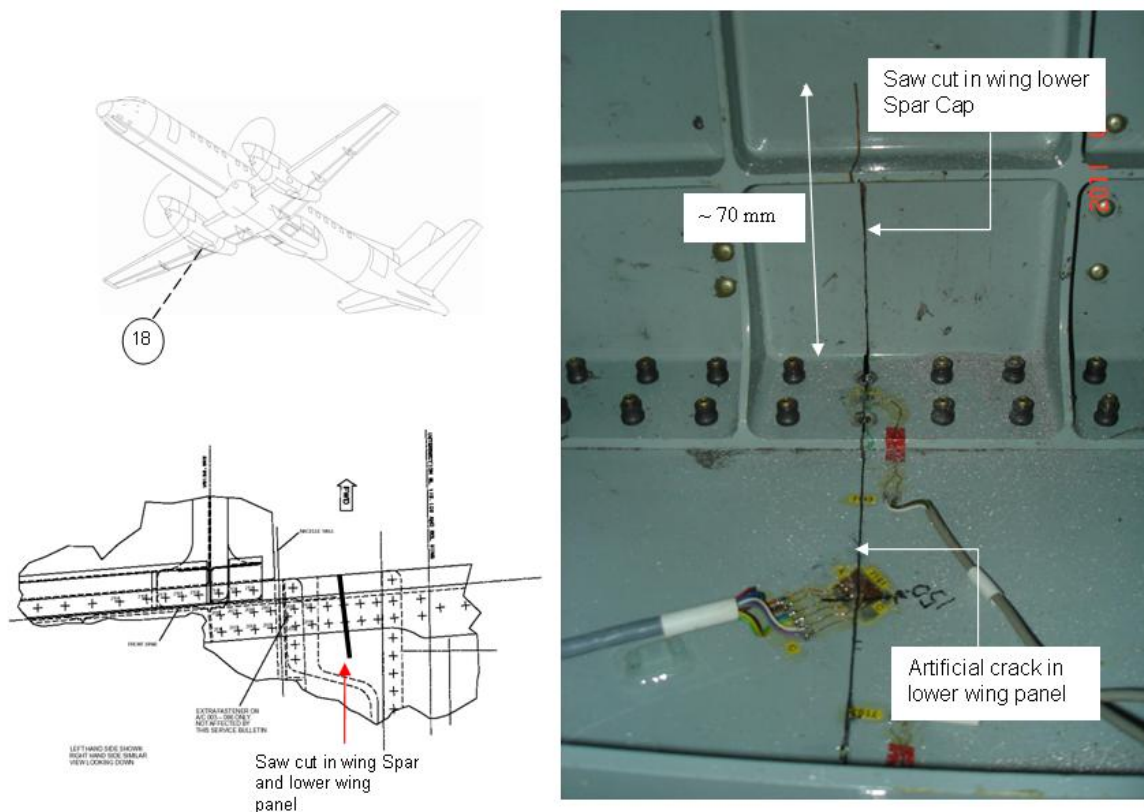


Figure 3.3.2-10 Location of the saw cut in the wing structure

On the basis of all the residual strength it is concluded that all separate tests comply with the associated requirements concerning residual strength capability. In plain language, it involves that all test cases fulfil the static strength up to limit load condition under three seconds without compromising the integrity of the elements.

All static residual strength tests were witnessed by an authority representative who granted all test cases in writing.

Subsequently, after inspection of the residual strength damages it was revealed that minor propagation of the artificial wing spar crack (figure 3.3.2-10 above) was observed. The crack was diverted in almost 45 degrees extending additional 20-25 mm.

#### Enlarged residual strength testing outside the basic certification program

As a part of an extending testing of the large damage capability, a final test of the pressurized fuselage hull was carried out. The aim with this test was to investigate and thereby find an upper limit for longitudinal cracks along rivet rows. This is relevant when adopting repair philosophies by using external repair doublers covering rivets through the existing skin panels.

The background for this originates from a request from the authorities to investigate the long term characteristics regarding structural repairs of primary structural elements. Thus, these repair evaluation guidelines from the authorities is now days reflected in part 26 DAH (Design Approval Holder) Rule announced by Federal Aviation Administration. The rule is interpreted as damage tolerance data for repairs and alterations.

The implementation of actions specified in repair evaluation guidelines is necessary to help ensure that the level of safety intended by the certification basis is maintained and that no unsafe conditions develop that might otherwise require specific mandatory action by EASA and FAA. Therefore airline operators whose maintenance programmes are approved under damage tolerance requirements should incorporate these repair evaluation guidelines into their maintenance programmes to address existing repairs and ensure they are damage tolerant and any necessary inspection requirements are implemented.

The subject test concerns a large longitudinal crack in the upper portion of the fuselage as given in picture 11. The artificial crack was located in an ordinary longitudinal splice between the side panel and the top panel and the test was carried out in two steps under internal pressure up to limit load condition. The limit load condition for testing represent a pressure level of 8.51 psi ( $\Delta p = 8.51$  psi). The normal operating differential pressure for Saab 2000 is 7.4 psi.

The first test was performed with a saw cut representing a crack of 30 inch (762 mm). Hence, at the subsequent test the artificial crack was extended to 35 inch (890 mm). This did not reveal any discrepancies; the pressure loading was sustained by the airframe without any secondary irregularities.

The second test involving the artificial crack of 890 mm was loaded up limit load pressure level ( $\Delta p = 8.51$  psi) under time corresponding to 3-4 seconds. Afterwards, a noise corresponding pulling rivets were noticed followed by a secondary failure in terms of sudden decompression of the fuselage. Figure 3.3.2-12 details the nature and the extent of the failure of the top panel of the fuselage. A large area of the upper portion of fuselage was ripped off resulting in a global failure covering a distance of approximately 170 inch (~ 4300 mm).

In conclusion, one interpretation from this test is that hidden cracks under for instance repair doublers may not be larger than 35 inch without compromising the overall structural integrity of the fuselage structure.

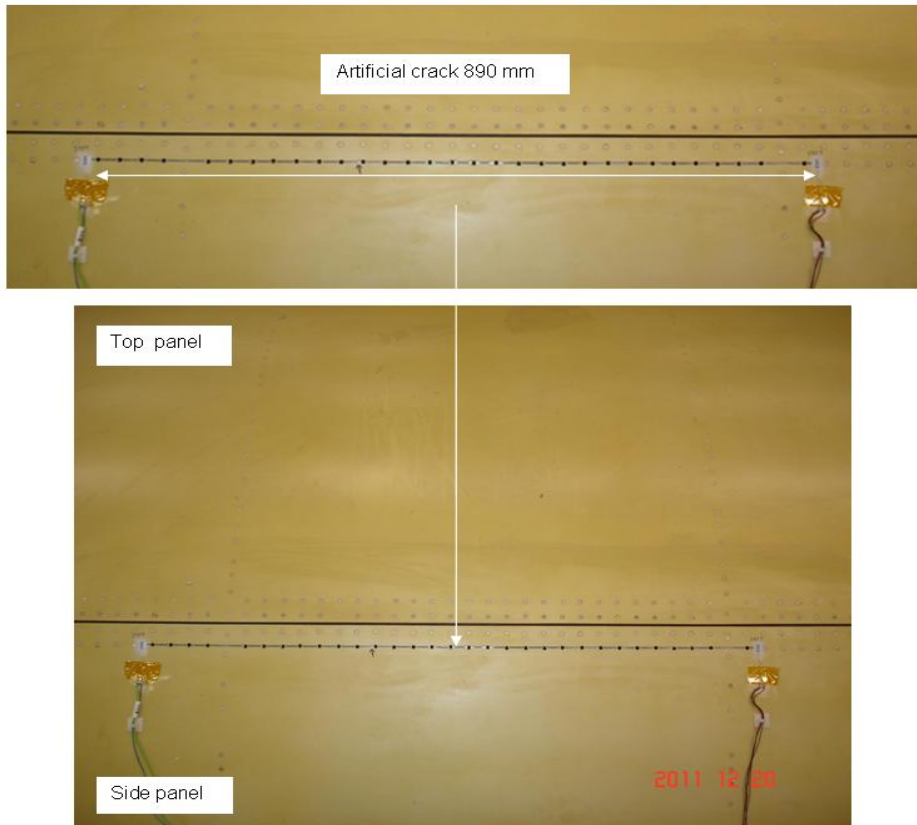


Figure 3.3.2-11 Location of the saw cut in the pressurized fuselage vessel



Figure 3.3.2-12 Final failure of the upper portion of the fuselage

### 3.3.3 JAS39 Gripen A/B/C/D Fatigue Testing

The strength verification programme with large components and complete airframes has been completed for versions A/B/C/D. The full scale fatigue test of the twin seater, 39B, was completed in 2000. The full scale fatigue test of the single seater, 39A, was tested much further in order to verify an extended life of the wing and fin of the C/D versions and was completed in 2007. The full scale fatigue test of a twin seater export version, 39D was completed 2008. Details about the test and results found during testing have been reported in previous Swedish ICAF reviews [1, 2]. The tear-down inspection programme for the 39A version has been completed and reported in the previous Swedish ICAF reviews [3]. The only remaining activity of these tests is the tear-down inspection of the 39D version which has after the main test programme been subjected to further testing of specific parts such as weapon pylon attachments, landing gear attachments, air-to-air refueling probe attachment. This additional testing has been completed and the tear-down inspection is underway.

### 3.3.4 JAS39 Gripen C/D Static strength test of pylons attachments in wing carrying heavy stores

Static tests have been performed with the purpose to verify static strength for the attachments of pylons 1, 2 and 3 in the wing structure. The test results have been used for strength assessment of carriage and separation clearance of heavy stores in pylons 2 and 3. The test results are also used for showing potential of load increase in the attachment structure for any future external stores.

The tests have been performed with a wing delivered from the Swedish Air Force. The wing was opened and furnished with strain measurement installations. A serial pylon 2 was used in the testing with a dummy structure attached to simulate the external loads from the stores. The same pylon 2 and dummy structure were used for both pylon station 2 and 3 testing.

Basic wing loads were applied in tip rib station, inner rib stations, outer flap attachments, elevon bearings. Pressurization of the fuel tanks was applied to simulate the dynamic pressure that occurs during flight maneuvers. Depending on which pylon station tested, 11 to 15 load channels used. Testing were made up and beyond 180% LL for a large number of flight, and store separation load cases for both pylon station 2 and 3. The measurements and tests outcome have cleared the operation of the heavy stores configurations considered.



Figure 3.3.4-1. Test setup with loading of pylon station 3.

### 3.3.5 JAS39 Gripen E test verification programmes for static, damage tolerance and fatigue life

The design work of the Gripen E version is in progress. The test verification of static strength and fatigue life will be made using two airframes including fuselage, fin and wings. Dummies will be used for flaps and elevons, canard, rudder, engine, landing gears, pylons (1-5), air intake, airbrake. Such parts will be tested separately. Excluded structural parts (not replaced by dummies) are radome, non-loadcarrying doors/hatches, landing gear doors, dorsal fin, fin fairing.

An actuator-rig is designed to apply actuator loads on the airframe such that global sectional forces are well represented, structure is not overloaded locally, actuator loads are distributed onto the airframe with a system of mechanical beams/bars, load introduction on the airframe using bonded pads or brackets using existing fasteners locations. The number of control channels is +130.

The same test rig (with some minor changes) will be used for both the static test airframe and the fatigue test airframe.

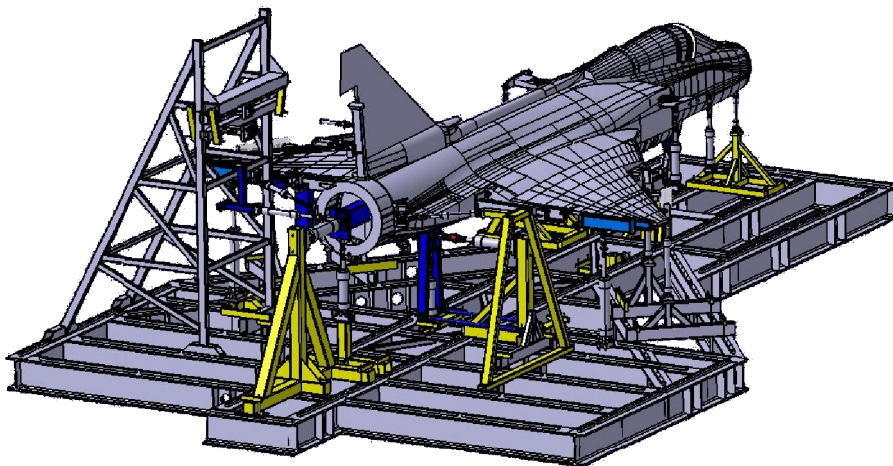


Figure 3.3.5-1. Test set up for the Gripen E full scale tests (work in progress figure not complete).

The static test article is planned to consist of the following test phases

- Testing to UL
  - in steps for selected load cases
  - UL = 150% LL for metal structures & 180% LL for composite structures due to environmental effects
- BVID impacts on composite structure
  - indent dept 1 mm or to cut-off energy 50J
- Simplified fatigue testing
  - selected significant load cases
  - extensive cycle elimination (30-50% LL)
  - no truncation of extreme loads
  - fatigue testing using LEF
- Residual strength test to UL = 180% LL
- Measurements of strain and impact damage sizes in all test phases
- Optional
  - overload test (above UL)
  - damage tolerance test (to LL or 120% LL)

The fatigue test article is planned to consist of the following test phases

- BVID impacts on composite structure
  - indent dept 1 mm or to cut-off energy 50J
- Strain measurements
- Fatigue testing
  - design spectrum
  - limited cycle elimination (~10% LL)
  - testing to 4 service lives
- Measurements of strain and impact damage sizes and NDT inspections at scheduled times during testing
- Measurements of strain and impact damage sizes in all test phases
- Tear down inspection

In addition to these full-scale tests of complete airframe, full scale damage tolerance tests of selected components will be made.

### 3.3.6 Damage Tolerance Test and Analysis of Wing Tip Pylons for the Gripen Aircraft

An updated airworthiness verification of the Gripen wingtip pylons by fatigue testing has been performed. The need for testing has been motivated by changes in operational profile and number of flight hours with stores carried in the pylons. Three pylons that have previously been used in service were submitted to fatigue testing in spectrum loading. In all three specimens, an early initiation and stable propagation of fatigue cracks was observed at stress critical locations.

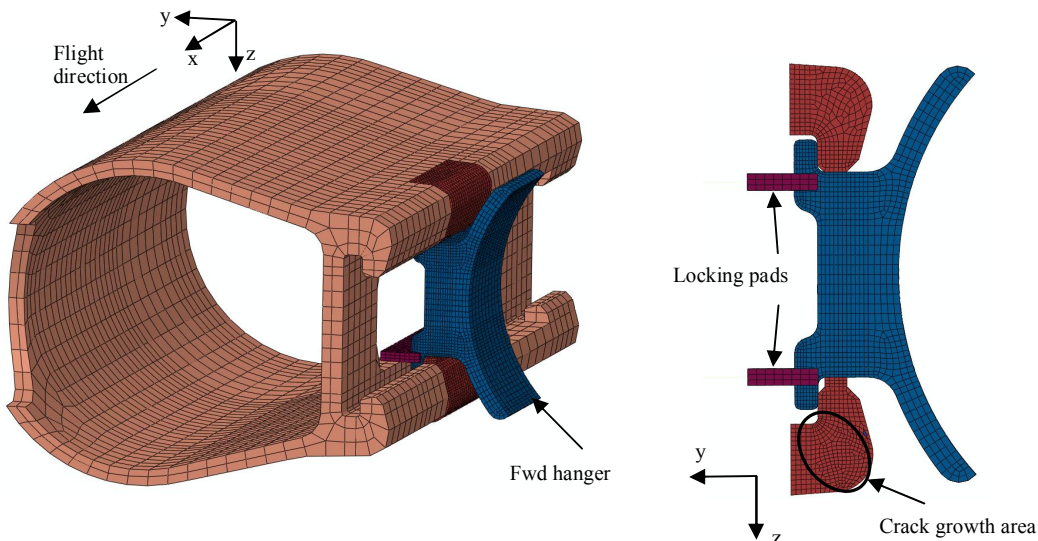


Figure 3.3.6-1. The fwd hanger area with the cut-through view of the hanger and the rail

The early initiation was attributed to the presence of corrosion pitting. Based on the testing results the allowable flight hours and inspection intervals are determined. To further support the testing results, analyses of the crack growth using the finite element software ABAQUS are performed. The extended finite element method capabilities of the software are used to represent the crack and obtain the stress intensity factor solutions for a three dimensional crack problem. The fatigue crack growth prediction is controlled by an iterative algorithm that produces the dependency of the stress intensity factor on the crack length. This relation is then used in AFGROW to perform the crack growth prediction which is then compared to the results from the testing, [4].



Figure 3.3.6-2. The fracture surface of test specimen and crack growth pattern in the analysis

### 3.3.7 Fatigue and damage tolerance aspects of hybrid metal-composite wing structures

The current trend in aircraft design is to increase the proportion of fibre composite structure. Since many primary structures still require to be constructed using metals, the number of interfaces between metals and composites increases. The structures containing both fibre composites and metals are referred to as *hybrid structures*. In the design and certification process of aircraft structures, such mixed structures have traditionally often been disregarded as an alternative because of the lack of methodology to handle the mismatch of material properties. With the growing number of hybrid structures, this problem needs to be addressed.

Some examples of differences between composite laminates and aluminum alloys are: thermal expansion coefficients, failure and fracture mechanisms, degree of plasticity, response to different types of loading i.e. tensile versus compressive and out-of-plane, fatigue accumulation and scatter, impact resistance, impact residual strength, degree of anisotropy, environmental sensitivity, density etc. Based on these differences, composite and aluminum materials used in aircraft structures are subject to different design and airworthiness requirements. The issues that therefore arise with hybrid structures are: thermally induced loads and deformations, multiplicity of failure modes in joints, characterization of damage in damage tolerant design, unanticipated structural failure modes, allowance for buckling and permanent deformations, determination of testing factors to account for material property scatter, determination of significant load states etc. From design point of view it is a challenge to construct a weight optimal hybrid structure where the right material is put into the right place.

Some common areas containing hybrid structures are found in particular in aircraft wing structures. Junction areas are usually composed of the outer shell of composite and the internal structures (spars, stringers and ribs) of metal.

The recommended practice for certification of composite assemblies, known as the Building Block Approach (BBA), is to conduct analysis and testing at various levels of structural complexity. Usually, a large number of small specimens are tested and analysed first, before progressing to more complex and expensive structural elements and finally ending with a full scale test. The knowledge gained at the previous levels is used as the base for designing the testing on the next level. This way, the risks in technology associated with complexity of composites may be uncovered and eliminated at an early stage.

When it comes to hybrid constitutions this approach may not always be appropriate, since the hybrid effects might be absent on lower structural levels. By this way of reasoning, the analysis and tests should be performed on a higher level first, in order to evaluate the hybrid nature of a structure and to discover the unanticipated structural behavior. Such testing can be very costly and a lot of understanding can be gained by performing detailed numerical analyses prior to the testing. In a recent Swedish project called HYBRIS, involving Saab, FOI and Swerea SICOMP, such research is conducted.

The aim of HYBRIS project is to assess the behavior of a hybrid wing-like box, with skins made of carbon fiber reinforced polymer (CFRP) and bolted to the inner structure made of aluminum, by testing and analysis. The material and geometry configuration of the object of study is based on the real wing structure of Gripen aircraft, see figure 3.3.7-1. It is built of C-shaped aluminum spars bolted to an aluminum splice section and covered with composite skins, figure 3.3.7-2. As can be seen from the figure, a large number of bolts are used to hold the structure together.

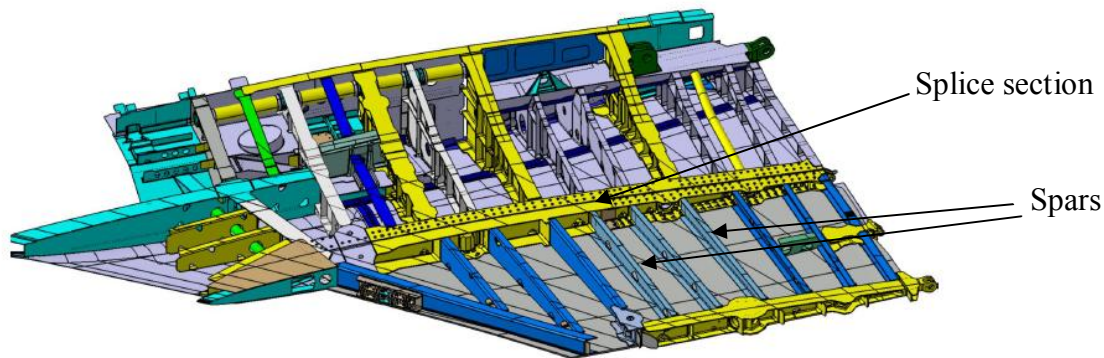


Figure 3.3.7-1. Inner wing structure of Gripen aircraft

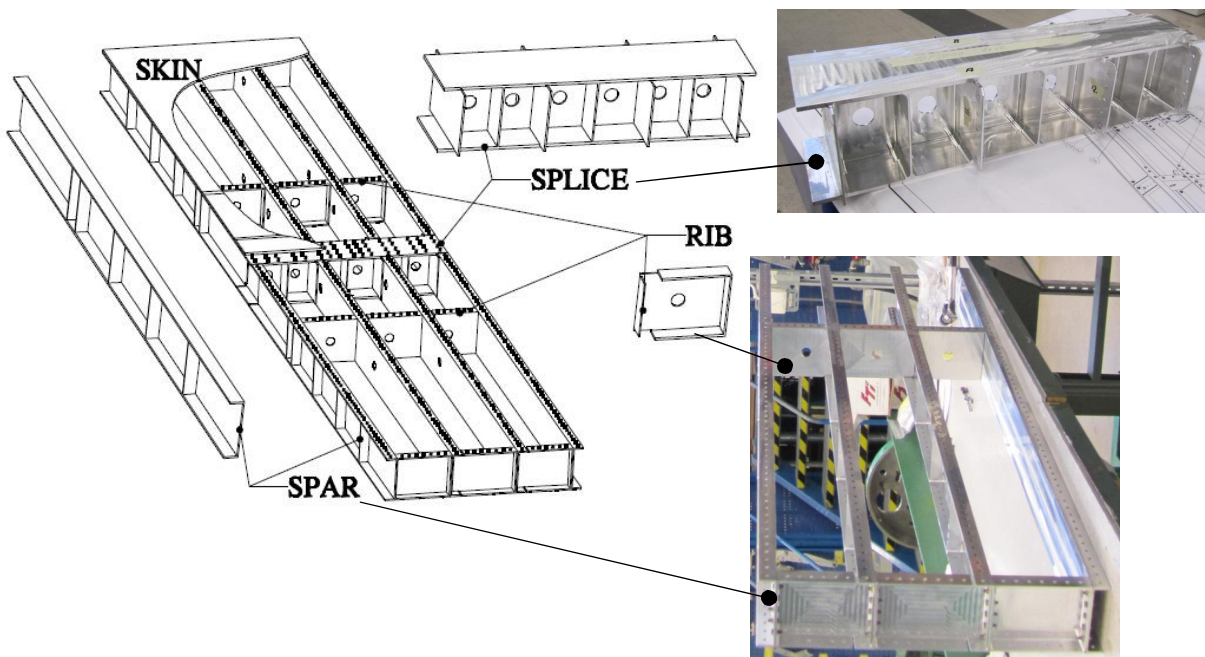


Figure 3.3.7-2. Inner structure of the test object in HYBRIS project, dimensions 3300x630x150 mm

The wing structure is normally exposed to bending and twisting operational loads and temperatures between -40°C and 80°C. To simulate this on the wing box, static and spectrum fatigue testing in a four point bending/twisting set up with an applied temperature is performed. Besides of its hybrid features, the wing box contains defects like artificial delaminations, low velocity impact damage and different types of ply drop-off regions.

The dimensioning requirements used for composites, currently used in the industry, are modified for the purpose of challenging the conservative assumptions and allowables. At the end of the testing program, the wing box will be filled with water and shoot at with small caliber bullet to test its battle damage resistance. The testing results are expected to indicate the critical features of the hybrid box from static, fatigue and damage tolerance point of view. Also, the influence of thermally induced loads on the structural behavior should be revealed.

Prior to the testing, the following analyses of the test object are performed:

- conceptual studies of different hybrid solutions and requirements
- dimensioning analysis
- local analysis of composite-aluminum bolted joints using FE
- FE analysis of low velocity impact
- FE virtual test simulation of the entire test object

### 3.3.7.1 Testing

#### Test object

The wing box test object has dimensions 3300x630x150 mm and is shown in figure 3.3.7-2. It consists of an aluminum inner structure of 8 spars, 6 rib sections and a splice section bolted to 4 CFRP composite skins. Countersunk titanium bolts are used. The skin lay-up is quasi-isotropic with lay-up sequence  $[(\pm 45/0/90)_n]_S$  in all 4 skins and each skin has 3 different regions with different thicknesses. The region where the skins cover the splice has a thickness of 8.32 mm, the area between the ribs and splice is 6.24 mm and the area outside the ribs is 7.28 mm thick. Between each area of different thickness, there is a ply drop-off region. These ply drop-off regions do not follow the rule that the thickness drop-off should be 1:20, instead different constitutions are tested. Also, artificial half circle shaped delaminations are inserted in the ply drop-off regions. In the middle of the upper skin (exposed to mainly compressive loads), impact damage is introduced by a spherical impactor and 50J of impact energy, see figure 3.3.7-3. Strain gauges are placed on the skin and in the inner structure in order to validate the FE-models and to calibrate the applied load.

#### Test set-up

The test object is placed on a rig, simply supported at both ends and on both upper and lower side. Mechanical loads are introduced by 4 actuators, via two steel frames that are clamped around the circumference of the box at rib locations, see figure 3.3.7-3.

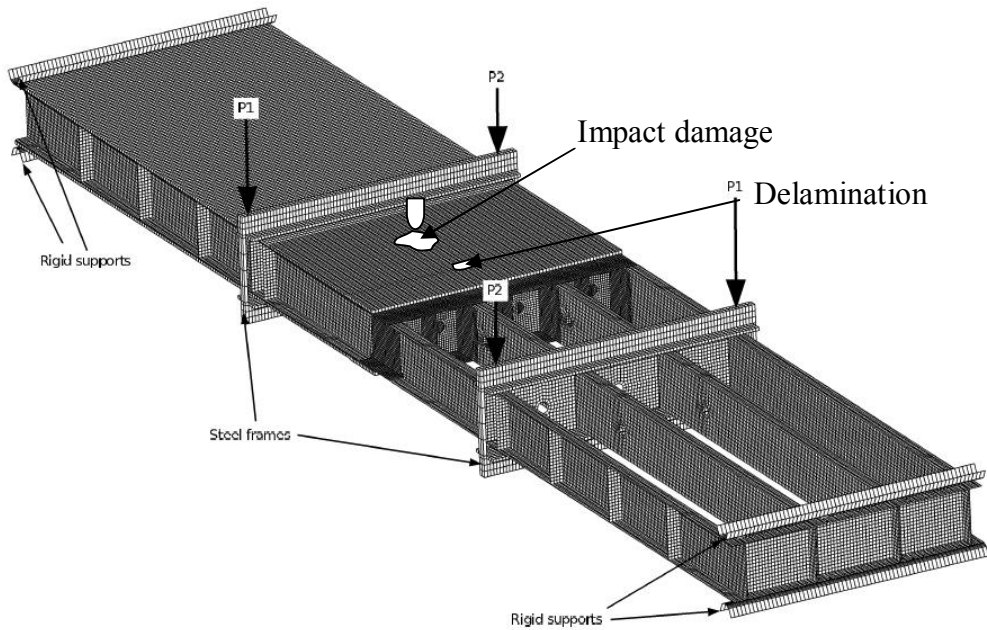


Figure 3.3.7-3. FE-model of the test rig up, with rigid supports and steel frames where the loads are introduced

Assigning the same loads to the actuators that are placed diagonally to each other gives a bending/twisting situation in the area between the ribs. A typical wing load spectrum is applied. The whole wing box is placed inside a furnace and a constant temperature of 70°C is applied throughout the fatigue testing. After the fatigue testing, the residual and static strength is tested on ultimate load level. The testing is planned to be performed during the spring of 2013 and finished in July.

### 3.3.7.2 Analyses

#### Conceptual studies of different hybrid solutions and requirements

Before designing the wing box, studies of two different hybrid concepts and two different requirement sets are conducted, [5]. Figure 3.3.7-4 shows a cross section of a spar-skin attachment for the two concepts studied and the baseline, an all composite design solution.

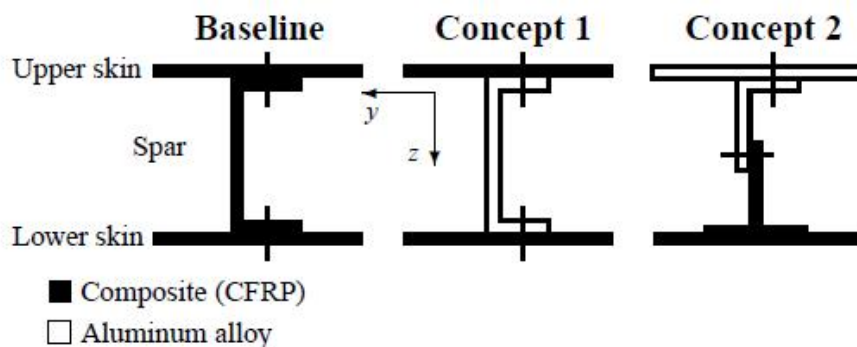


Figure 3.3.7-4. Skin-spar attachment for an all composite (Baseline) design, Concept 1 (C1) and Concept 2 (C2) designs

In the conceptual study, the design solutions from figure 3.3.7-4 are applied to a wing box without a splice section, i.e. only two composite skins and 4 spars, see figure 3.3.7-5. No considerations are taken to impact damage and delaminations.

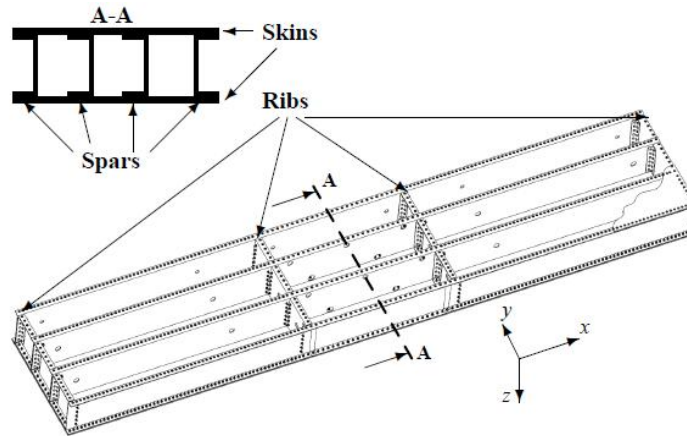


Figure 3.3.7-5. Wing box used in the conceptual study

The conceptual study is done as follows. First, the baseline concept is designed applying the currently used design requirements for composites and typical wing skin dimensions. The dimensioning loads of the baseline are then applied on the two hybrid concepts and the resulting weights are compared. Next, the process is repeated using a modified set of composite design requirements.

The two design requirement sets include the following considerations:

*Set 1*

- Fiber controlled and balanced laminates
- Environmental influence, i.e. temperature and moisture, considered
- Fastener joints and cut-outs considered
- No buckling allowed below ultimate load level
- Allowable strains determined by utilizing damage tolerance design and considering 6 mm hole everywhere in the laminate
- No-growth concept (on delaminations) utilized by the 6 mm hole requirement
- Structure is required to sustain temperatures between  $-50^{\circ}\text{C}$  and  $90^{\circ}\text{C}$

*Set 2*

- Fiber controlled and balanced laminates
- Environmental influence, i.e. temperature and moisture, considered
- Fastener joints and cut-outs considered
- Buckling allowed above 1.2 times the limit load level
- Allowable strains determined by utilizing damage tolerance design and considering the risk of impact occurrence and damage
- Structure is required to sustain temperatures between  $-30^{\circ}\text{C}$  and  $70^{\circ}\text{C}$
- The influence of battle damage assessed by simple assumptions

The conceptual study revealed that the dimensioning criteria were onset of buckling and bolt failure if buckling is allowed. In aluminum parts, low margins against fatigue were obtained. The influence of thermally induced loads on the structural behavior was found to be entirely different in the two concepts. Concept 1 had the lowest weight in both requirement sets and was chosen to be used in the design of the test object.

### Dimensioning analysis

The test object was dimensioned against the new requirement set using analytical and numerical (FEM) methods. In contrast to the conceptual study, the aluminum splice section is now included into the wing box. However, the impact damage and the artificial delaminations are not taken into consideration in the dimensioning calculations.

The outer dimensions of the wing box were determined beforehand, so the dimensioning calculations were mainly concerned with the determination of thicknesses and lay-ups, bolt dimensions and local stiffeners against buckling in the area of load introduction. It turned out, that the critical sites, both statically and fatigue-wise, were the single lap shear bolted joints in the area of the splice section. Based on the dimensioning calculations, the magnitude of applied mechanical ultimate and spectrum loads to be used in testing are determined. For fatigue calculations, the applied temperature is set to 50°C and maximal temperature statically is set to 70°C at ultimate load.

#### Local analysis of composite-aluminum bolted joints using FE

Since the dimensioning calculations pointed out the bolted joints in the splice section as the critical sites, special attention was directed to these parts, [6]. The tool used in dimensioning analysis of the composite bolted joints is Saab in-house program Cobolt. This program assumes and solves a two-dimensional stress field in the vicinity of the bolt hole and evaluates bearing and net-section failure criteria.

In order to gain deeper understanding in the three-dimensional nature of the problem of bolted joints, FE-analyses are conducted. Commercial FE software Abaqus is used for modeling and solving. A three dimensional, solid element FE-model of the shear loaded joint shown in figure 3.3.7-6 is developed. The model includes a countersunk titanium bolt with contact and friction, bolt pretension effects, a plasticity model for metal and a progressive damage model (PDM) for composite. The progression of the bearing failure is captured by degrading the stiffness properties of the composite at a material point when a certain stress based failure criterion is met. For this purpose, an Abaqus subroutine called USDFLD is written and included into the FE-model.

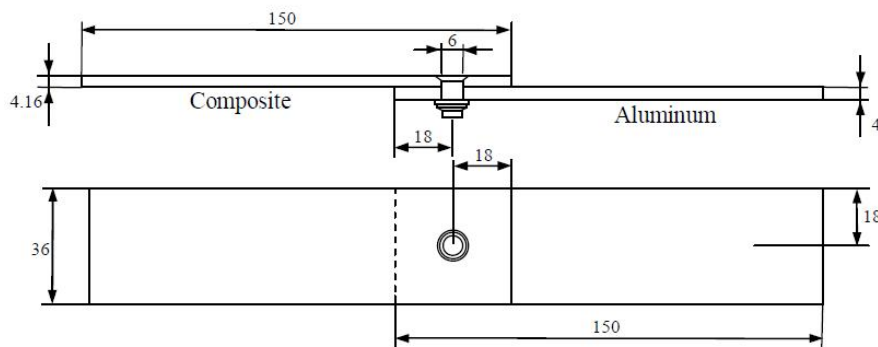


*Figure 3.3.7-6. Hybrid composite-aluminum single lap shear joint with a titanium bolt.*

The resulting strains and force-displacement characteristics are compared to the experimental results with the same joint. Figure 3.3.7-7 shows the stresses and the force-displacement comparison. In figure 3.3.7-8, the bearing damage in the countersunk composite plate is shown.

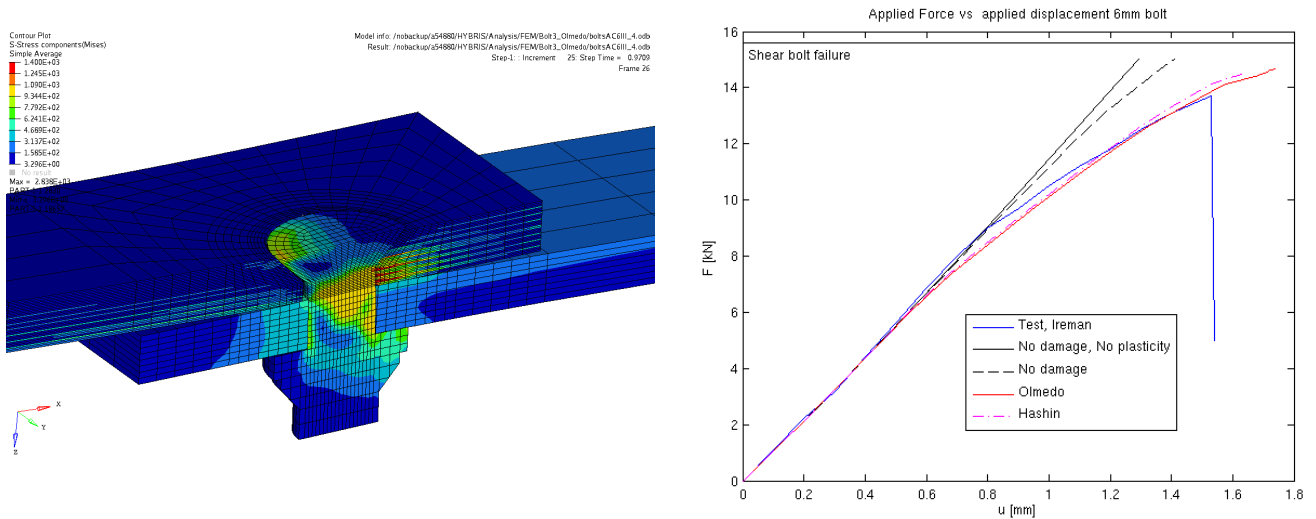


Figure 3.3.7-7. Stress distribution in the joint and comparison of force-displacement characteristics between the analysis and experiment

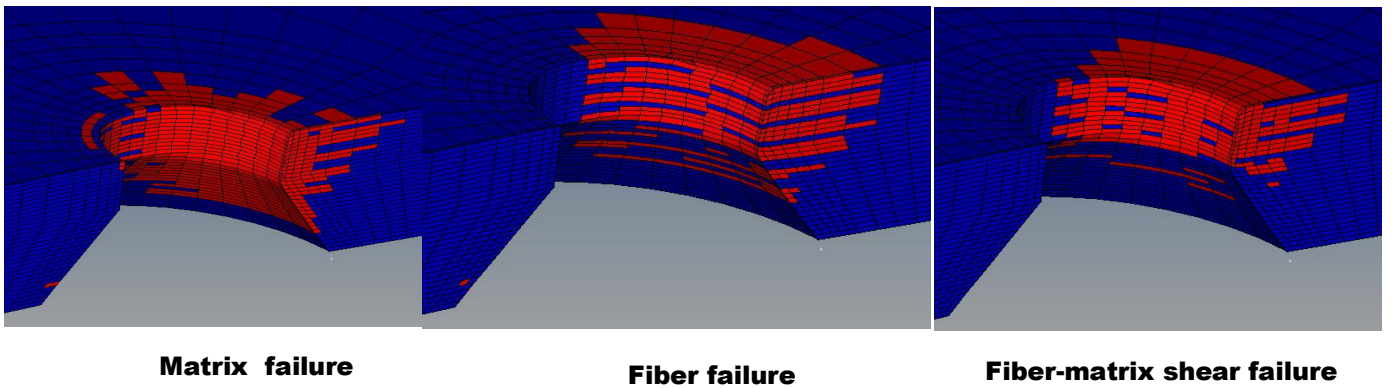


Figure 3.3.7-8. Bearing damage in the composite plate

### FE analysis of low velocity impact

In the scope of damage tolerant approach to composite design, low velocity impact is one of the most important issues. In this detailed analysis of the impact event, a solid FE-model of the impacted composite skin between the ribs and the splice, see figure 3.3.7-3, is developed using Abaqus, [7]. Each ply is modeled with one solid element through thickness and the 5 kg spherical impactor weight is modeled as a rigid surface. Intralaminar failure is included into the model via a VUMAT subroutine.

To capture the interlaminar failure, i.e. delamination, during the impact event, cohesive elements are placed at every ply interface. The failure in these elements is governed by a simple traction-separation law which takes into account multiple fracture modes. Once the fracture energy in the element is consumed, the element is removed from the model allowing the ply-interfaces to be separated. The progress of the impact is solved by the central difference algorithm in Abaqus/Explicit.

The results of a typical impact simulation and experiment (from literature), in terms of force-time history, force-displacement and delamination patterns are shown in figure 3.3.7-9 and 3.3.7-10.

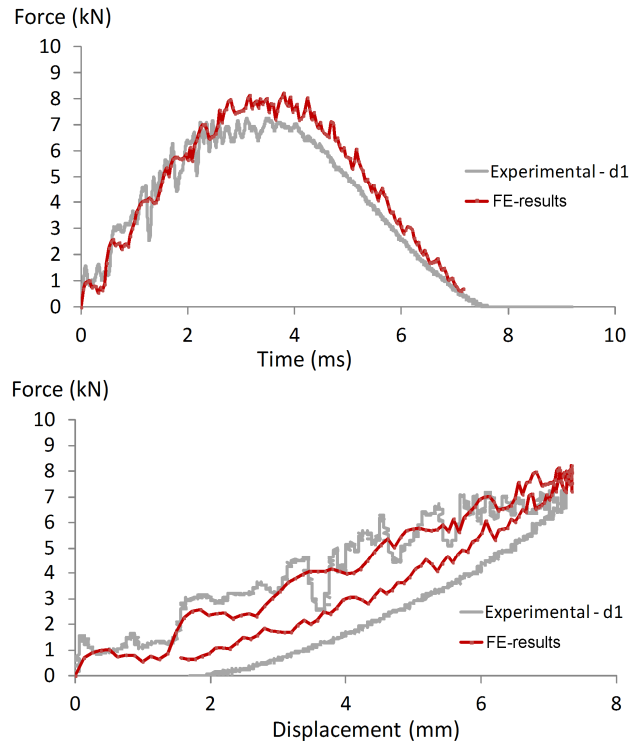


Figure 3.3.7-9. Comparison of simulation and experimental results found in the literature

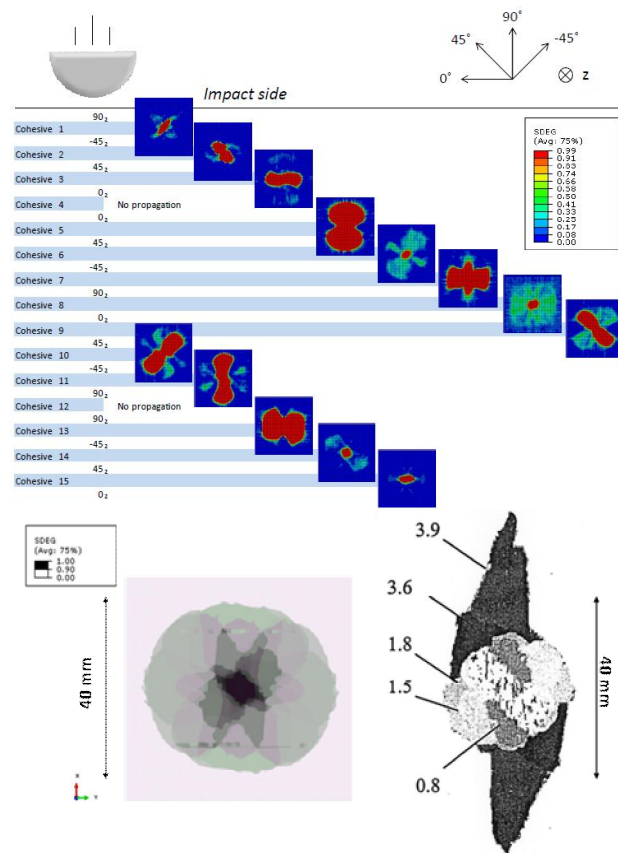


Figure 3.3.7-10. Delamination patterns in each ply interface and in the whole laminate compared to C-scan measurements on the same laminate from the literature

### FE virtual test simulation of the entire test object

The structural behavior of the entire wing box and the experimental set up is modeled using Abaqus, see figure 3.3.7-3. The boundary conditions, corresponding to the supports at each end of the box, are modeled as rigid bodies with half-spherical cross-section, which are in contact with the box. Also the steel frames, where the actuator loads are applied, are modeled with contact to the box. For representation of the composite skins, one continuum shell element with stacked formulation is used through the thickness. That means that each ply is represented as an integration point within a single element. For aluminum parts, ordinary shell elements are used. Contact conditions are enforced between all included parts and the model is solved using Abaqus/Standard implicit solver.

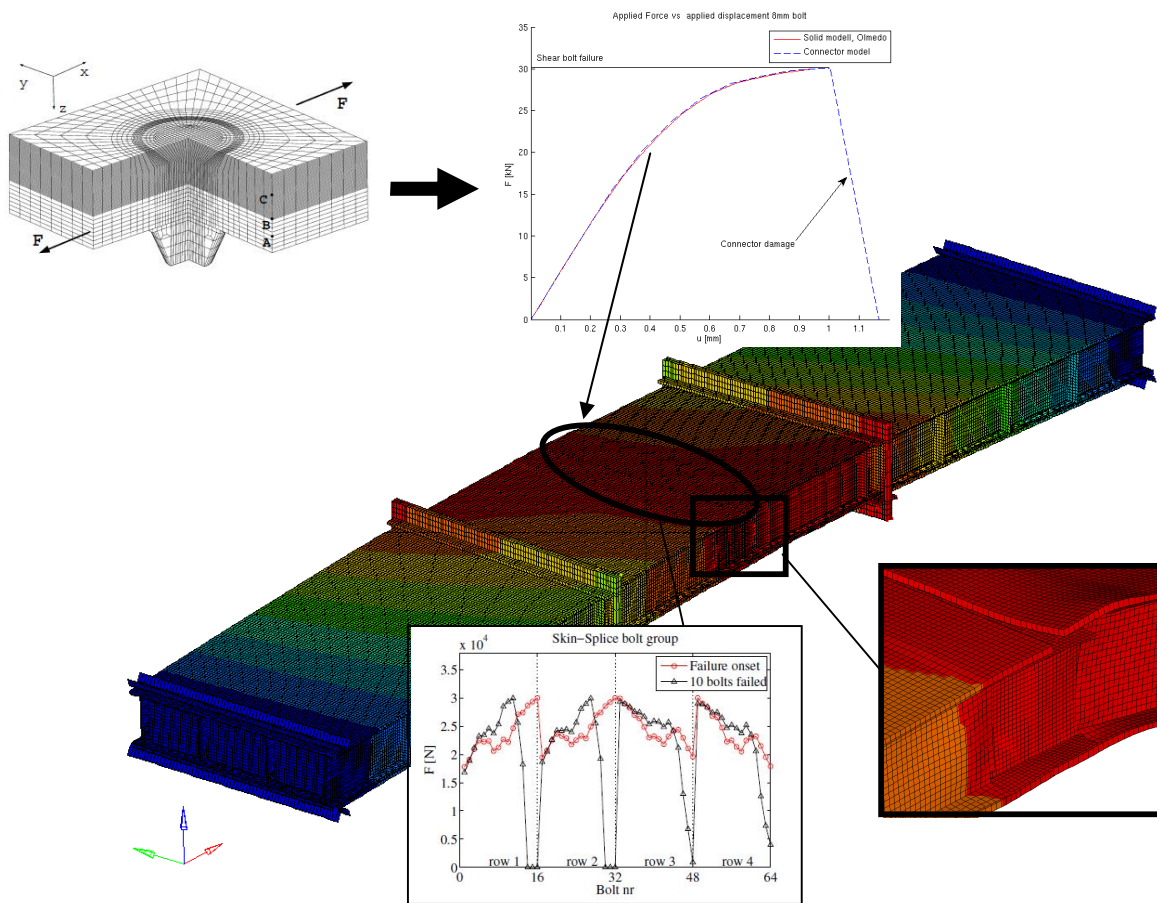


Figure 3.3.7-11. Extracting the force-displacement behavior from a local solid model, assigning the behavior to connector elements and solving the global structural model with fastener load redistribution

All bolts in the structure are represented by two-node connector elements available in Abaqus. These elements can be chosen to have different number of degrees of freedom and can be assigned a large variety of constitutive behaviors. In this case, elements with six degrees of freedom per node are chosen and elasto-plastic behavior with damage accumulation and failure is assigned to them. With behavior is meant a force-displacement curve similar to the one in figure 3.3.7-7, only applied to the shear resultant force. These curves are extracted from local solid models, as the one described previously. When the load reaches the level where the shear failure of the fastener is expected, the load is rapidly reduced to zero. Assigning such behavior to structural elements allows for studies of load redistribution due to composite damage, metal plasticity and fastener failure. This is illustrated in figure 3.3.7-11 for the case of the studied wing box.

The remaining part of the analysis work is to include the impact damage obtained by a local model into the global structural model. The residual strength of the box can then be obtained by monitoring the growth of the impact delamination in the upper skin. In order to solve the problem Abaqus feature co-simulation, which couples implicit and explicit solving techniques might be used. The impact area would then be solved by explicit solver and the rest of the box by the implicit.

Also, the evaluation of testing and comparison to the results from analyses remains to be done.

### 3.4 FATIGUE CRACK INITIATION AND PROPAGATION

#### 3.4.1 A parametric fatigue life prediction method for generic aircraft fitting

The current investigation is aiming to generate an easy-to-use design tool for parametric studies of generic aircraft fittings. The objective is to rapidly obtain the stress field around the critical zones by FEM. Two different generic shapes will be analysed: T-joints and Bath-tub joints, see figure 3.4.1-1.

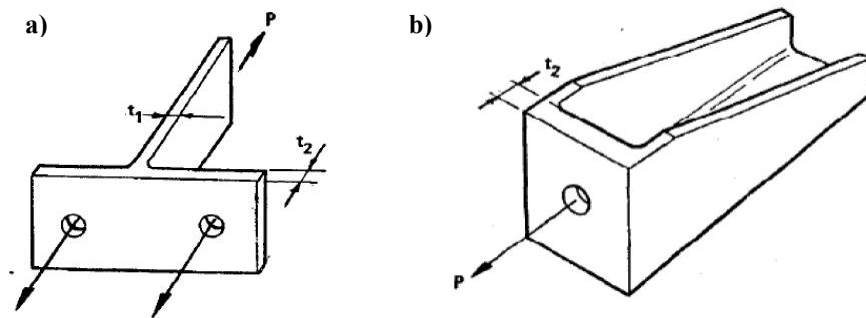


Figure 3.4.1-1. a) T-joint. b) Bath-tub joint.

The critical areas are located in the zones of maximum bending moment due to the offset between the bolt location and the force 'P' application point, see figure 3.4.1-1 and 3.4.1-2. That area is characterized by a transition radius which induces a high stress concentration. Those sections that suffer a sever load state will become the triggers for fatigue crack formation under cyclic load if not proper design has been done.

The main parameters involving the study are: bottom thickness ( $t_1$ ), end plate thickness ( $t_2$ ), radii at intersection of plates, flange thickness (for bath-tub type), and pretension of the bolts, see figure 3.4.1-1. Due to the strong dependence of the stress field on the boundary conditions of the problem; the contact between the bolt, the washer and the plates needs to be modelled, see figure 3.4.1-2a.

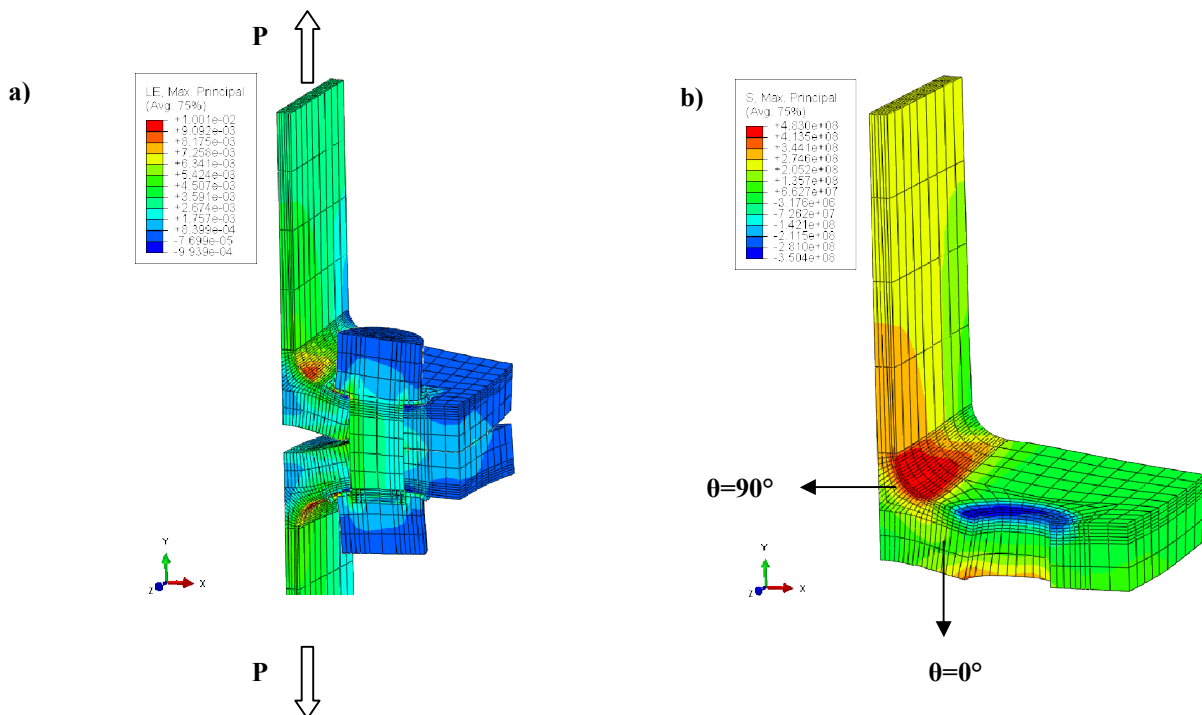


Figure 3.4.1-2. a) Maximum principal strain distribution of the model plate-bolt-washer for the T-Joint. Units in [m/m] b) Maximum principal stress distribution in the critical radius and angle orientation reference used in figure 3.4.1-3. Units in [Pa]

A significantly fine mesh is required for the contact surfaces and the critical radius zone in order to achieve non-dependent mesh results. This fact considerably increases the required computational time. The material model for plasticity is taken into account in order to get good correlation with experimental data. There exist a variability of results and uncertainty introduced by the friction coefficient between the contact surfaces. This fact forces the problem to consider the friction coefficient as an extra parameter in the analysis, see figure 3.4.1-3. In order to reduce the parameters involved, an average friction coefficient is considered in the study.

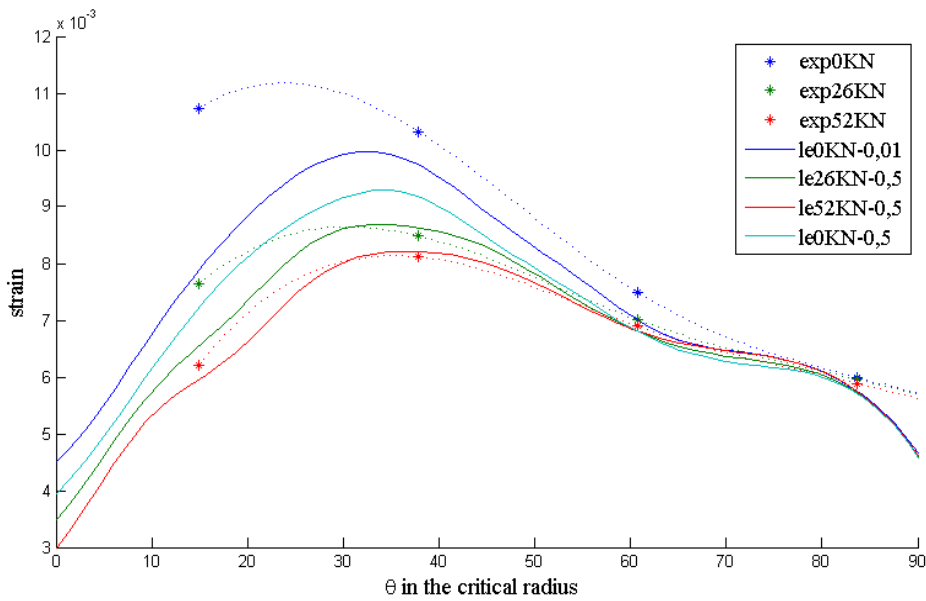
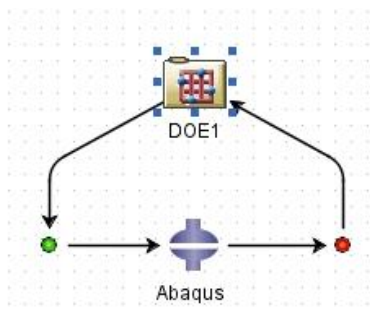


Figure 3.4.1-3. Maximum principal strain distribution along the critical radius for different bolt pretension loads (0KN-26KN-52KN) and different friction coefficients (0,01-0,5). Comparison between experimental data (asterisks smoothed by dotted lines) and FE-results (continuum lines). See figure 3.4.1-2 for θ orientation reference. Units in [m/m].

The validation of the model is achieved according to the variability of strain distribution due to different boundary conditions given by different pretensioned bolts, see figure 3.4.1-3.

In order to manage such huge amount of simulations and data, an Isight model is developed through the integration of a Design of Experiments (DOE) block, Abaqus, a parametric geometry and a parametric mesh in the interest of externally manage all the parameters involving the study case. By using the described procedure the speed and efficiency of the whole process is significantly increased, see figure 3.4.1-4.



FrictCoef	radi_tjoint	t1_tjoint	t2_bolt	t2_tjoint	S_maxprin_max
0.1	0.0010	0.0030	0.01	0.01	5.39181E8
0.1	0.0030	0.0030	0.01	0.01	4.96119E8
0.1	0.0050	0.0030	0.01	0.01	4.73761E8
0.1	0.0070	0.0030	0.01	0.01	4.59237E8
0.1	0.0090	0.0030	0.01	0.01	4.51396E8

Figure 3.4.1-4. Isight model simulation flow diagram and design matrix. Units in [m] and [Pa].

After the validation, the parametric model is launched in order to explore the design space of the generic fitting, see figure 3.4.1-5.

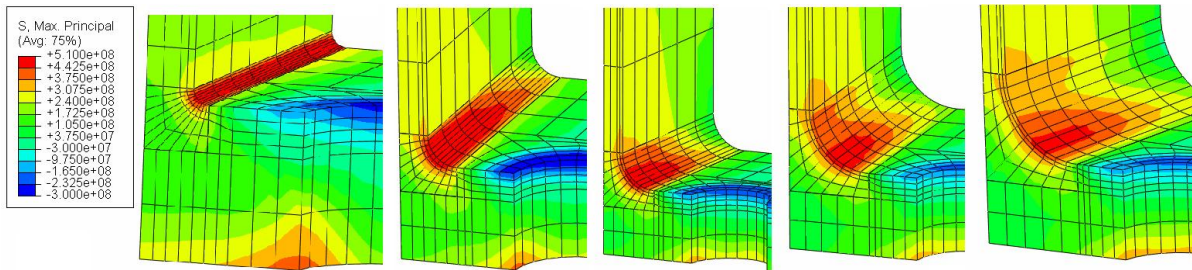


Figure 3.4.1-5. Comparison of maximum principal stress distribution for different generic geometry variations according to the design matrix shown in figure 3.4.1-4 Units in [Pa]

Also the stress intensity factor distribution is aimed to be obtained by the introduction of semi-elliptical cracks in the model, see figure 3.4.1-6.

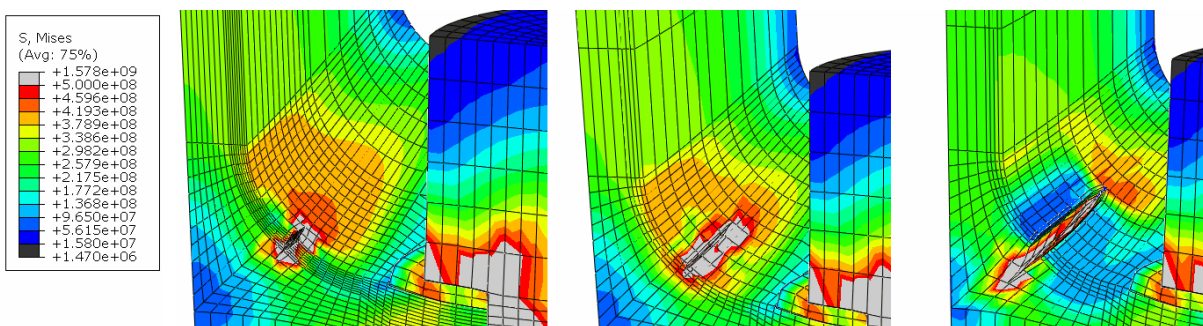


Figure 3.4.1-6. Stress field for different crack lengths and crack aspect ratio Units in [Pa].

Fatigue life prediction will also be performed in order to crosscheck the results obtained with the experimental spectrum fatigue testing available. The results shown will also be obtained for bath-tub shape generic fittings in order to get an accurate idea of the fatigue and damage tolerance design space for aeronautical application fittings.

### 3.4.2 Modelling of high temperature fatigue crack growth in Inconel 718 under hold time conditions

Inconel 718 is a frequently used material for gas turbine applications at temperatures up to 650°C. For such components, the main load cycle is typically defined by the start-up and shut-down of the engine. In this main loading cycle, hold times at high temperature are generally present for critical components. These high temperature hold times may greatly increase the fatigue crack growth rate with respect to the number of cycles, and it has been shown that this anomalous behaviour is due to material damage in the crack tip vicinity causing the material to fail by intergranular fracture [8-10]. Between these hold times different types of loadings can occur e.g. sections/blocks of continuous cyclic loading. These can be caused by abnormal service conditions but can also occur on a more regular basis due to e.g. different weather conditions and engine vibrations. It has been shown previously that not only the crack growth rate during the hold times but also the cyclic crack growth is affected by the material damage [8]. Thus, it becomes important to understand the interaction between

hold times at high temperature and cyclic loading conditions in order to model the behaviour of e.g. real engine operation cycles.

The high-temperature hold times give rise to an embrittlement that causes intergranular fracture. The mechanisms of the hold time effect affect a volume of material around the crack tip, here referred to as the damaged zone, which gets a lowered resistance to fatigue crack propagation compared to the unaffected material, see e.g. [8] and also [11] for further discussions on the mechanisms behind the hold time effect.

### Modelling

Modelling of the hold time fatigue crack growth behaviour of Inconel 718 in the time dependent region and at the temperature  $550^{\circ}\text{C}$  has been carried out by using the concept of a damaged zone, where scale factors depending on its length are used for accelerating both the cyclic and hold time parts.

In detail the following additive law is proposed

$$\left(\frac{da}{dN}\right)_{\text{total}} = \left(\frac{da}{dN}\right)_{\text{cyclic}} + \left(\frac{da}{dN}\right)_{\text{time dependent}}$$

where

$$\left(\frac{da}{dN}\right)_{\text{cyclic}} = S_c(D) \cdot \left(\frac{da}{dN}\right)_{\text{baseline}} = S_c(D) \cdot C_c(\Delta K)^{n_c}$$

and

$$\left(\frac{da}{dN}\right)_{\text{time dependent}} = \int_{t_{\text{hold}}} S_t(D) \cdot \left(\frac{da}{dt}\right)_s dt = \int_{t_{\text{hold}}} S_t(D) \cdot C_t(K_{\text{hold}})^{n_t} dt$$

where the labelling “c” and “t” refer to cyclic- and time-dependent quantities, respectively and where the label  $s$  indicates stabilized time dependent crack growth. Furthermore, the labelling “baseline” refer to behaviour under standard testing, i.e. cyclic loading with a sufficiently large frequency for which no damaged zone has time to evolve. Finally,  $S_c$  and  $S_t$  are monotonically increasing scaling functions of the current length of the damaged zone  $D$  and, finally,  $C_c$ ,  $n_c$ ,  $C_t$  and  $n_t$  are positive constants in the Paris law expressions.

It is to be noted that the usage of a scaled baseline-term implicitly implies the assumption of sufficiently rapid load reversals. However, although the damaged zone is continuously growing during the hold times the crack is also growing, but usually in a much slower rate, see figure 3.4.2-1. Furthermore, if a block of cyclic loading would be imposed, the damaged zone is progressively destroyed, see figure 3.4.2-2. Thus, the total rate of the evolution of the damaged zone will depend on two parts,  $\dot{m}$  and  $\dot{a}$ , forming a combined rate.

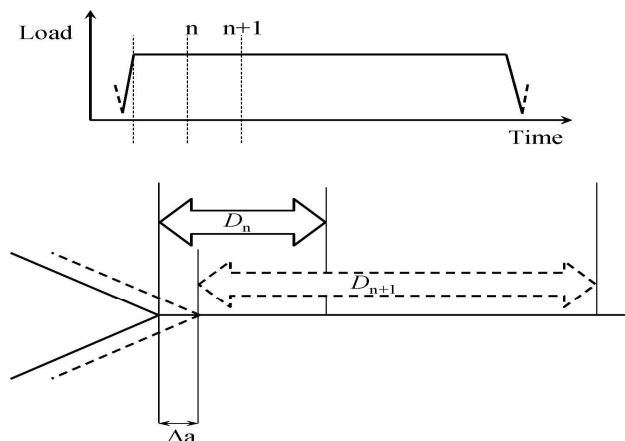


Figure 3.4.2-1: Build-up of damaged zone

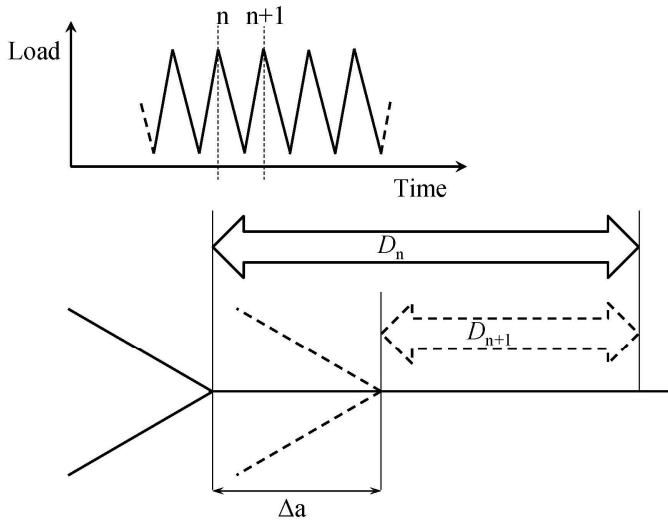


Figure 3.4.2-2: Destruction of the damaged zone

Based on the adopted time dependent crack propagation description, it is here proposed that

$$\dot{D} = \dot{m} - \dot{a}$$

$$\dot{m} = C_{\tau} K_{\text{hold}}^{n_{\tau}}$$

where  $\dot{m}$  represents the mechanism based growth rate of the damaged zone.

With this choice of evolution equation for  $D$ , in combination with the assumption of a monotonically increasing scaling function  $S_{\tau}$ , the evolution of  $D$  will be stable in the sense that  $D$  will never be larger than the value for which  $S_{\tau}$  reaches unity.

Since the frequency for the pure cyclic loading is assumed high, the mechanisms based crack growth during the load reversals can be neglected, thus implying

$$\frac{dD}{dN} = - \frac{da}{dN}$$

Finally, the laws controlling  $S_{\tau}$  and  $S_c$  are to be set up. The first,  $S_{\tau}$ , controls to what extent the damaged zone affects the hold time part, see Eq. , and should e.g. be able to describe the transient from pure cyclic loading to a block of hold times, see figure 3.4.2-3.

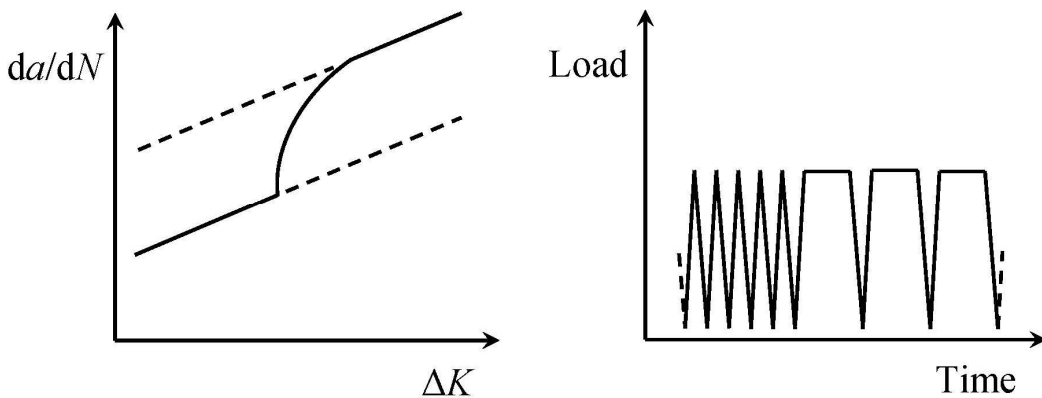


Figure 3.4.2-3: Acceleration of the fatigue crack growth with increased damaged zone length

Since,  $S_z$  is to be a monotonically increasing function of  $D$ , and since it for the case of no damaged zone should be zero, it may be given the form found below, where  $B_z$  is a fitting parameter.

$$S_z = \left( \frac{D}{D_{\max}} \right)^{B_z} \quad B_z \geq 0$$

More complex expressions involving more parameters are of course possible to conceive, but in order to keep the description as simple as possible, and in order to introduce as few parameters as possible, the above expression was chosen. Please note that the quantity  $D_{\max}$  corresponds to the measurable length of the damaged zone under stabilized time dependent crack growth.

The second factor,  $S_c$ , controls to what extent the damaged zone influences the cyclic part, and should e.g. be able to describe the transient from a hold time block to pure cyclic loading, see figure 3.4.2-4.

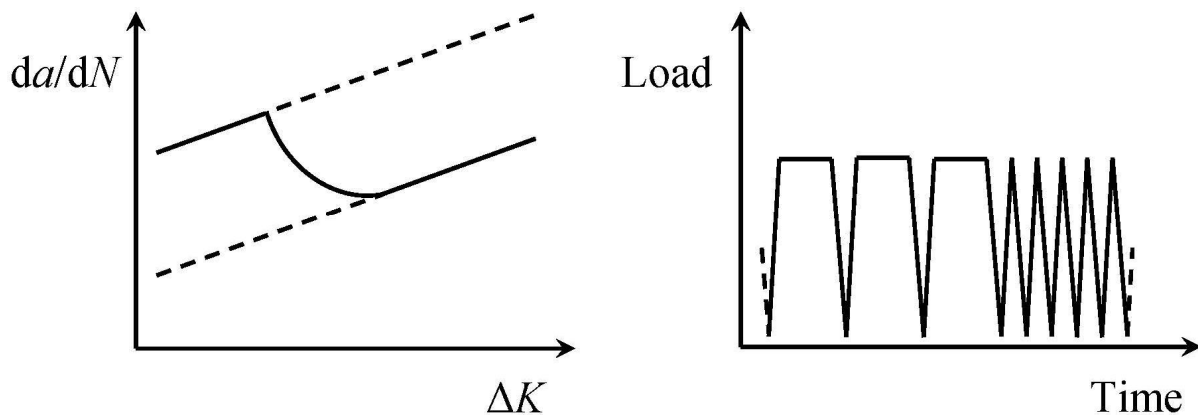


Figure 3.4.2-4: Acceleration of the fatigue crack growth with increased damaged zone length

Since  $S_c$  is to be a monotonically increasing function of  $D$ , and since it is to take the value one for the case of an “undamaged” crack-tip material, it may be given the form shown below, where the two fitting parameters  $A_c$  and  $B_c$  have been introduced

$$S_c = 1 + A_c \left( \frac{D}{D_{\max}} \right)^{B_c} \quad B_c \geq 0$$

Again, the simplest possible choice of expression has been chosen in order to keep the model as simple as possible.

With the chosen evolution laws for  $S_c$  and  $S_z$ , all crack growth rates will lay in between the pure cyclic fatigue crack growth rate and the pure time dependent crack growth rate. As one can see from the model expression,  $S_z$  will only reach its maximum value of one for sufficiently long hold times, which corresponds to pure time dependent crack growth, i.e.  $D = D_{\max}$ . The opposite applies for  $S_c$ , starting at a high value depending on how close  $D$  is to  $D_{\max}$ , and slowly decreasing towards its minimum value of one as the damaged zone is completely “consumed”.

### Results

The proposed model contains a small set of fitting parameters which can be found from basic experiments. Below, a few examples of the model results are given. As can be seen in figure 3.4.2-5 the 2160 s and 21600 s hold time tests are captured reasonably well.

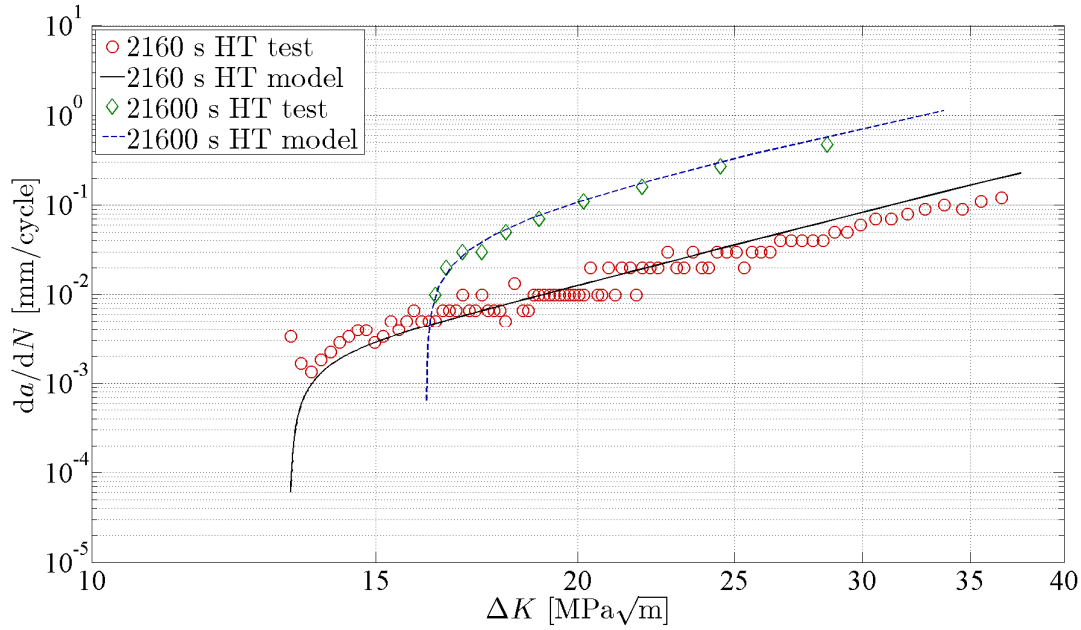


Figure 3.4.2-5: Model vs. hold time tests

As an example of the model output for crack length vs. time, the result for the 21600 s hold time test is shown in figure 3.4.2-6. As can be seen the model captures the overall behaviour of the test satisfactorily.

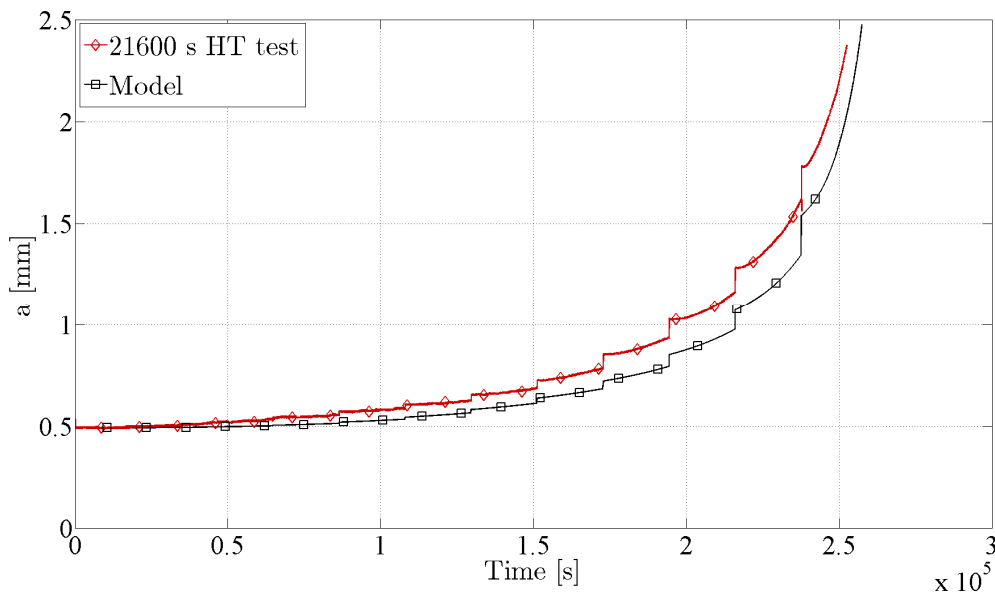


Figure 3.4.2-6: Crack length vs. time for the 21600 s hold time test

### 3.4.3 Topology optimization with respect to stress and fatigue

Structural topology optimization is a first optimization step which mainly is used for finding conceptual designs in early design stages. The main difference between topology optimization and other structural optimization techniques is that no initial design is required. The optimization is instead started from a block of material which is limited by the allowable design space. A fixed finite element mesh is used and each element is assigned a design variable, which determines if the element should represent a hole or structural material. An optimized conceptual design, which satisfies the given

constraints and connects the applied loads to the given supports, is automatically obtained by the optimization.

Traditionally, topology optimization has been used for finding the stiffest structure for a prescribed amount of material. This formulation is computationally efficient but does not necessarily yield a design which is feasible with respect to the structural requirements that the part will be subjected to. Research has therefore been devoted to topology optimization where the objective is to find the lightest possible design which also satisfies structural requirements in terms of stress and high-cycle fatigue, [12].

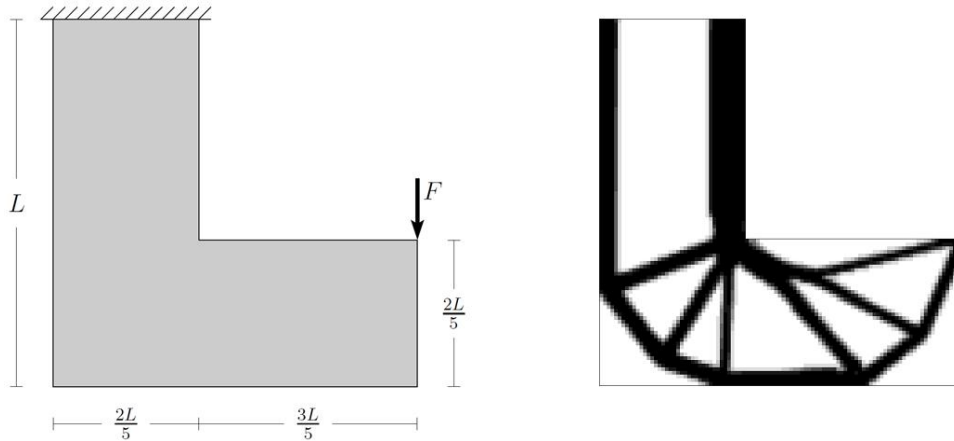


Figure 3.4.3-1. Test example: “L-shaped beam”. Design domain to the left and optimized design to the right.

The main difficulty with stress and fatigue in a topology optimization is that they are local measures, i.e. a failure will occur if the stress becomes too high in any point. Local constraints in topology optimization, e.g. one constraint for each finite element, give a very large problem which becomes too expensive to solve. However, it is not possible to select a number of critical spots to constrain; these are not known *a priori* since there is no initial design. A clustered approach [13] has therefore been developed, in which a small number of constraints are applied to clustered stress measures which approximate several local stresses.

The fatigue analysis that is used for the optimization is simplified and the aim of using fatigue as a constraint is not to replace a final fatigue analysis, but to find a design which not has to undergo severe modifications in later design stages. The fatigue constraint is based on that the part is designed for a specific number of flight hours according to a given load spectrum and the damage for each load pair is accumulated according to Palmgren-Miner’s rule. With some assumptions about the structure, as discussed in [12] and [14], the highest stress (critical fatigue stress),  $\bar{\sigma}^f$ , that gives an allowable cumulative damage,  $\bar{D}$ , is sought by solving  $(P_{crit})$ . The fatigue analysis is here represented by operators  $S_l$ , which represent scaling a stress for a unit load by the load levels in the spectrum and operators  $H_l$ , which represent reading the allowable number of cycles from the Haigh diagram. The problem  $(P_{crit})$  reads

$$(P_{crit}) \left\{ \begin{array}{l} \max_{\bar{\sigma}^f} \bar{\sigma}^f \\ s.t. \quad \sum_{l=1}^L \frac{n_l}{H_l(S_l(\bar{\sigma}^f))} \leq \bar{D}, \end{array} \right.$$

where  $L$  is the number of load pairs in the spectrum and  $n_i$  is the actual number of cycles for each load pair, as given by the load spectrum. The critical fatigue stress is then used as a stress limit in the topology optimization, where local principal stresses are grouped into clustered stress values, which then are constrained.

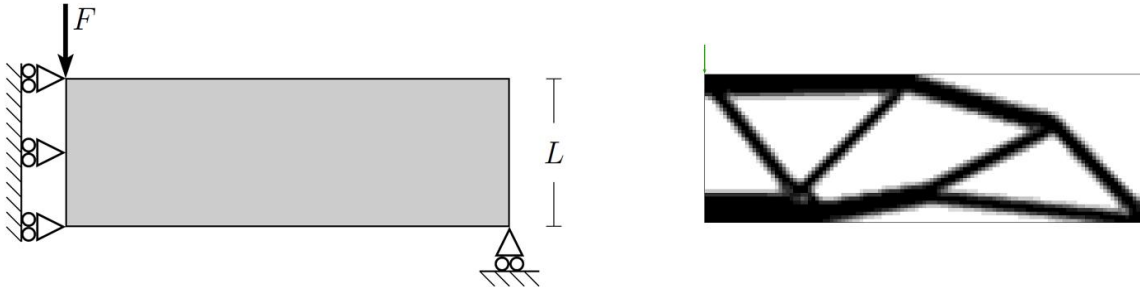


Figure 3.4.3-2 Test example: "MBB beam". Design domain to the left and optimized design to the right.

The methodology has been verified on well known academic test examples in 2D. For industrial applications, the optimization methods must be applicable to 3D-structures. Future work on this subject will therefore focus on 3D, which not only raises the question of how to formulate a simple fatigue constraint, but also increases the computational cost substantially; thus, also requires more efficient calculations. This may be accomplished by the use of faster algorithms and parallel computing, but it is also necessary to decrease the number of constraints and design variables in a way that do not limit the design. Some suggestions were given in [12]: for example, as fatigue cracks usually initiate at the surface, the fatigue constraints may be applied only to elements which in the current iteration are close to a surface. Further, design variables which not are expected to change in the current iteration may be deactivated so that the expensive sensitivity analysis not has to be made.

The 2D-problems and the optimized designs, obtained by minimizing the mass subjected to constraints on static stress and high-cycle fatigue, are seen in figure 3.4.3-1 and figure 3.4.3-2. Compared to the traditional stiffness based optimization, more mature designs are obtained when stress and fatigue constraints are employed; large stress concentrations are avoided and the structural parts are sized with respect to the allowable static stress limit and the critical fatigue stress.

### 3.5 COMPOSITE MATERIALS

#### 3.5.1 Biaxial testing of composite joint

More and more composites are used in aircraft structures and somewhere the composite will be joined to aluminium. Those joints often use fasteners and they will have composite on one side and aluminium on the other side. Carbon fibre composites for aircraft structures often have a thermal expansion coefficient close to zero while it for aluminium is fairly large at  $23 \cdot 10^{-6} \text{ K}^{-1}$ . Composite structures are subjected to a wide range of temperatures, very low temperatures due to operation in an arctic climate or flying at high altitude, and high temperatures due to operation in warm climate or frictional heating from flying fast at low altitude. An elevated temperature will cause the aluminium to expand more than the composite in a mixed joint. The fasteners will transfer thermal loads causing the composite to expand and the fasteners at the edges will take the largest thermal load. In figure 3.5.1-1 is a schematic of the thermal loads on the composite part in the mixed joint, horizontal forces, and mechanical loads, vertical forces. To simulate this load case on a composite a small specimen was designed, see figure 3.5.1-2. The mechanical force is in the vertical direction and has the same magnitude on both fasteners. The thermal load is simulated by applying a mechanical load in the horizontal direction. The load on the composite hole surface in the specimen is then similar to that on the hole surface to the right in the mixed joint, see figure 3.5.1-1. But, a two fastener joint is much cheaper to manufacture than a large joint with many fasteners.

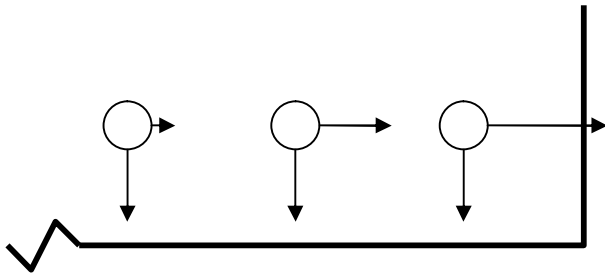


Figure 3.5.1-1 Schematic of thermal and mechanical loads on composite part in a mixed joint at elevated temperature

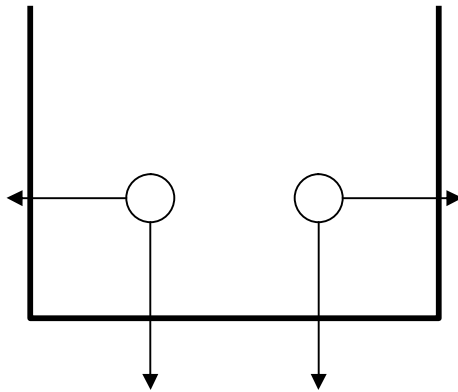
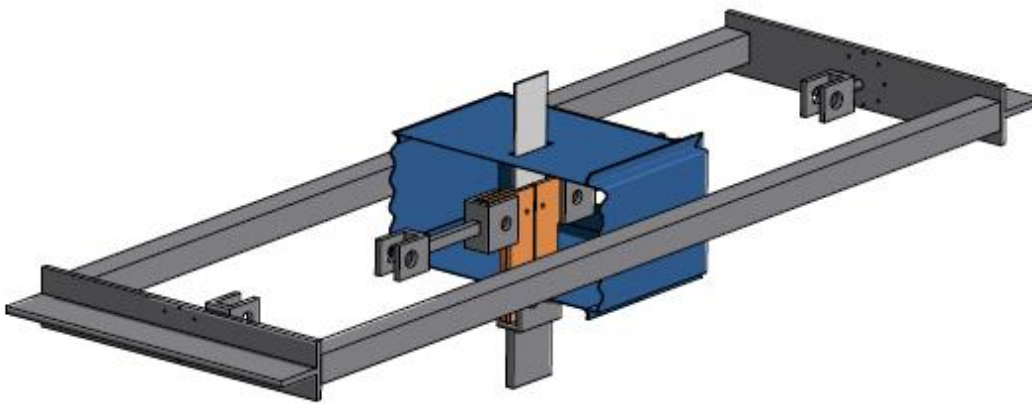


Figure 3.5.1-2 Schematic of load on composite specimen

To implement this load case, a biaxial testrig was designed which can be used in an ordinary load frame, see figure 3.5.1-3. The specimen is light grey and vertical in the figure and it is

inserted in grips of a load frame. Each fastener is connected by a plate on each side, orange, as in a double lap specimen. Those plates are connected vertically by bushings to a plate which is inserted in the grips of a load frame. In the horizontal direction the plates are joined with bushings to rods. Those arms are joined with bushings to hydraulic cylinders and load cells to apply horizontal force and measuring the force. The hydraulic cylinders and load cells are not shown in the figure. A steel frame is connecting the two hydraulic cylinders. It is hanging in springs and can move both horizontally and vertically without any problems. This causes the horizontal load to be equal on both sides and any horizontal forces are avoided in the vertical load frame. The specimen is placed inside an oven, blue in figure. In the vertical load frame grip displacement and force is measured. In the horizontal direction force and hydraulic cylinder movement is measured.



*Figure 3.5.1-3 Fixtures for biaxial testing*

Testing has begun on 8 mm thick specimens with 8 mm fasteners tightened to a little more than 1 Nm, fingertight. The specimens are heated to 90 °C and constant amplitude loaded in the vertical direction. An example of grip displacement versus number of cycles is shown in figure 3.5.1-4. The change in biaxial grip displacement, upper curve, is fast at beginning of testing and then the rate of change becomes constant. At a point the biaxial grip displacement begins to increase quickly and the specimen breaks after that. In figure 3.5.1-5 is a picture of the specimen after failure and the failure mode is bearing failure and the influence from the biaxial load is clearly shown. The vertical grip displacement decreases with increasing number of cycles. This might be due to that the biaxial loading causes bearing failure to continuously create a “new hole” for the fastener with a good fit. Early fatigue results suggest that biaxial loading will decrease fatigue life.

The test programme is ongoing, a total of 80 test specimens of the same design and material are available for testing. The main number of specimens will be tested under spectrum loading with different levels of peak loads clipping and extreme peak loads addition. The basic spectrum is FALSTAFF. Aluminium specimens (AA7010) of the same design are also included in the test programme. These specimens will be tested under similar spectrum modifications.

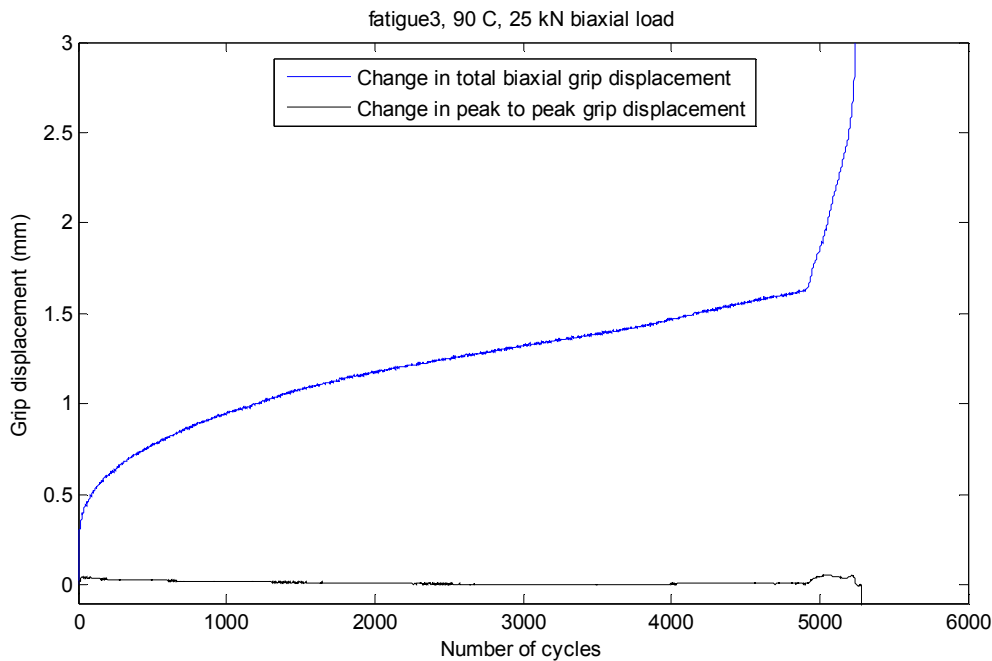


Figure 3.5.1-4 Grip displacement versus number of cycles



Figure 3.5.1-5 Biaxially loaded specimen after failure.

### 3.5.2 Detailed measurements of bearing failure in composite bolted joint

A single lap composite joint with one fastener has been studied, [15]. The first objective was to develop an optical method to measure rotation of bolt and plates in a single bolt composite shear lap joint. The second objective was to understand the correlation between bolt rotation in a joint and the failure load. To do this, three aluminum plates with a speckle pattern was glued to both plates in the joint and to the bolt head. The specimen was inserted in a load frame and loaded slowly to failure. During loading two cameras photographed the aluminum plates. The translation of the aluminum plates were calculated using digital speckle photography techniques. By comparing the translation of the aluminum plates when the joint was loaded with when it was not loaded the rotation of the aluminum plates was calculated. Since the aluminum plates were glued to the joint composite plates and bolt head the rotation

of the composite plates and bolt was measured. Bearing stress was then plotted against bolt rotation and grip displacement. A transition bearing stress was defined as the stress where the slope of the curve changed. Ten different joints were tested.

Figure 3.5.2-1 show how the different parts of the joint rotate for a 64 plies joint. The bolt rotation is as expected the largest one. The rotation of the plates is due to the secondary bending that occurs in almost all cases, even if the free length was as small as it could be. When damage begins to form at the bolt the rotation of the plates begins to deviate.

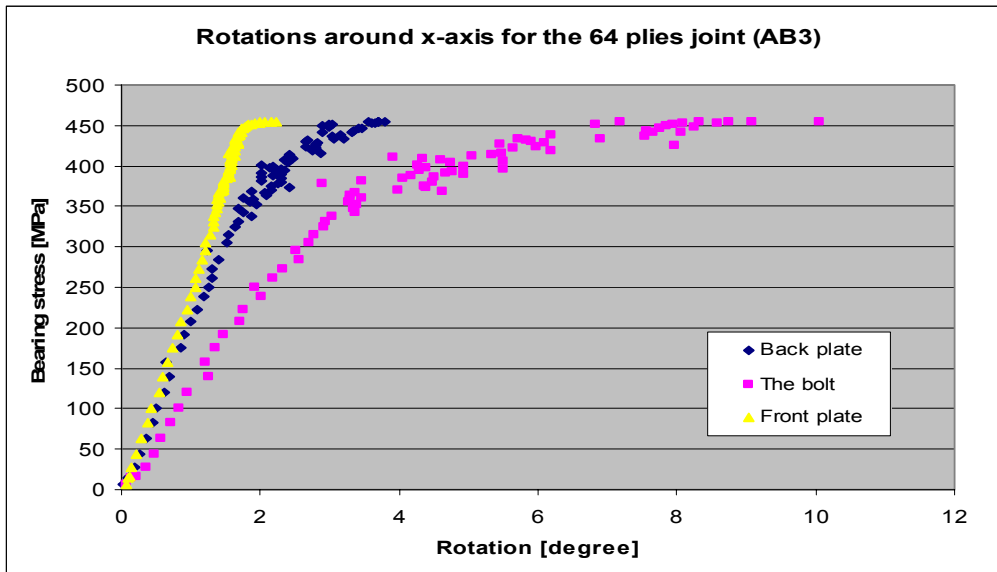


Figure 3.5.2-1 Typical chart of bearing stress vs. rotation of both bolt and joint plates. (64 plies joint)

Figure 3.5.2-2 shows the correlation between bearing stress and bolt rotation. The 24, 48, 64 plies joints show that for 24 plies the maximum bearing stress is highest and the bolt rotation gets as high as 24 degrees. As the joint-plate gets thicker, 46 plies, the maximum rotation and bearing stress drop. The more the bolt rotates the more load will be transferred through the bolt by tensile loading instead of shear loading which is usually the case. The joint breaks when the bolt breaks.

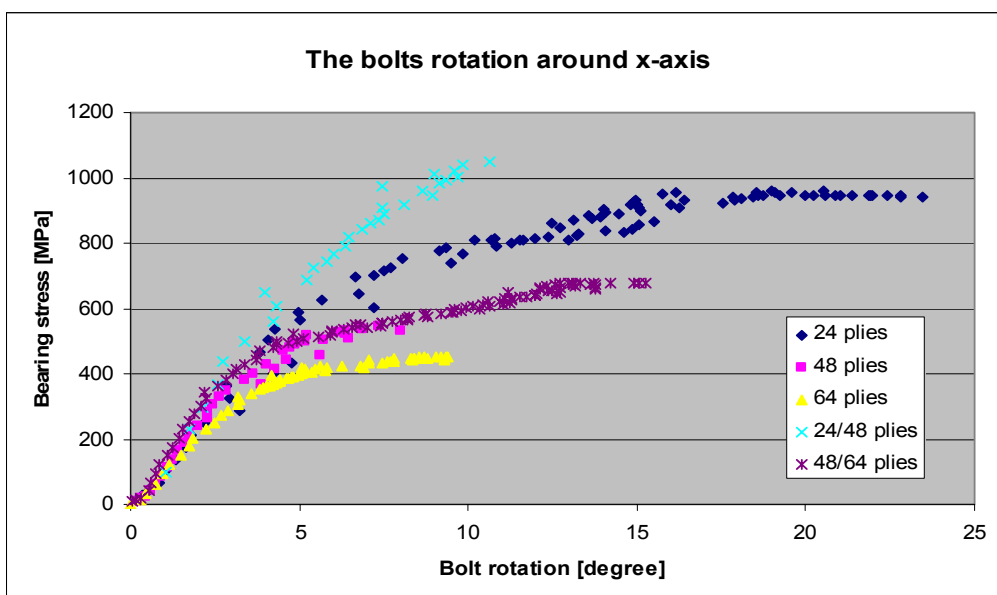


Figure 3.5.2-2 Bearing stress versus bolt rotation for the five joints with different thicknesses.

Increased free-length gives an increased secondary bending, see Figure 3.5.2-3. This makes the joint more resistant to bearing failure and increases both the transition bearing stress and bolt rotation at failure, the last one from 20 degrees to 25 degrees. Measuring the rotation of the front plate in a joint could be an alternative method to measure secondary bending in a joint.

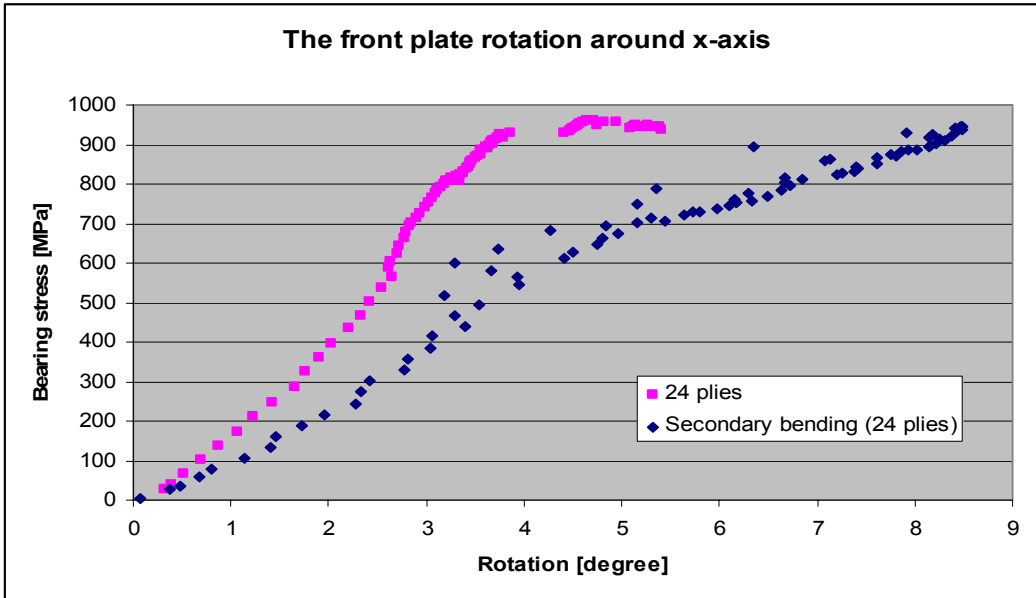


Figure 3.5.2-3 Bearing stress versus front plate rotation for two joints with different length.

The bolt rotation at transition bearing failure has been divided with the corresponding bearing stress. When calculating the bolt rotation, the rotation of the front plates was subtracted. The obtained value is the slope in a bearing stress versus bolt rotation figure. Then these values have been plotted against transition bearing stress to tell if there is a correlation.

Almost all of the values follow a line in figure 3.5.2-4, proposing that a correlation exists. The more bolt rotation per applied bearing stress, the lower the stress value of transition bearing stress. This indicates that the more easily the bolt rotates, the lower the transition bearing stress.

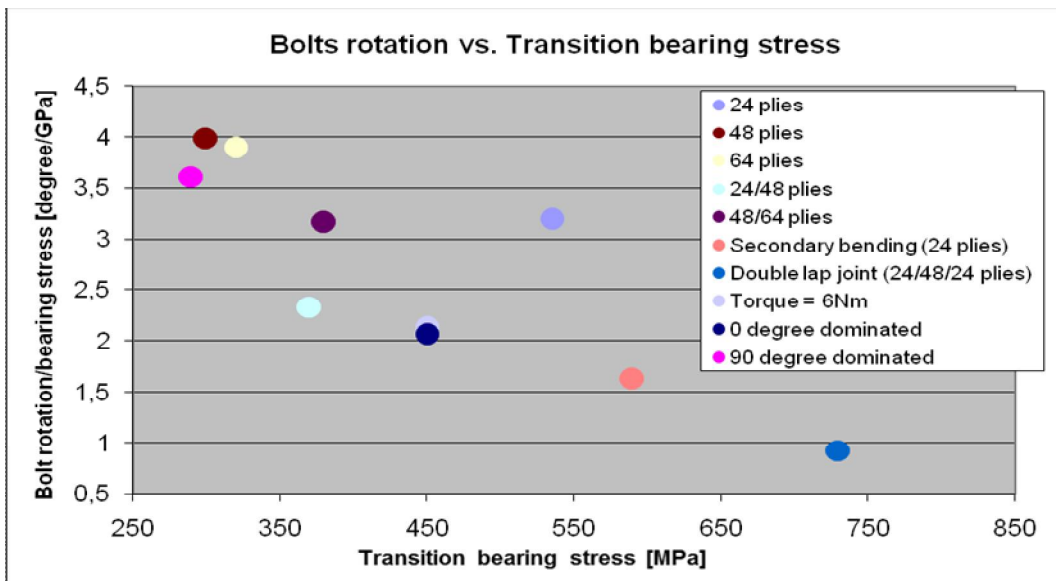


Figure 3.5.2- 4 Correlation between bolt rotation and transition bearing stress

In figure 3.5.2-5 the maximum bearing stress has been plotted against transition bearing stress. The results suggest that a higher transition bearing stress gives a higher maximum bearing stress.

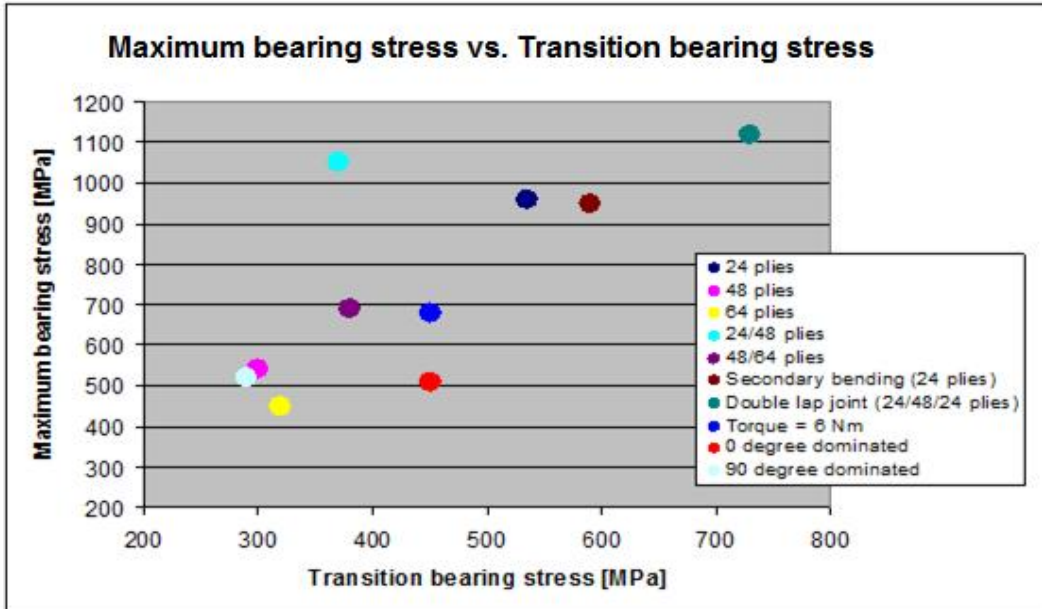


Figure 3.5.2-5 Maximum bearing stress versus transition bearing stress.

### 3.5.3 Enhancing structural efficiency through novel dissimilar material joining techniques (SAFEJOINT)

There is a high demand for the design of lightweight energy efficient structures for transport applications in order to meet CO<sub>2</sub> emissions targets set worldwide. To achieve this designers have introduced the concept of “hybrid” structures where two or more lightweight materials are used each possessing unique properties that when joined together result in high performance lightweight structures that would not have been possible if a single material was used. This approach requires the development of joining techniques for materials with fundamentally different physical properties that will ensure the safe and reliable transfer of load between the constituent materials.

SAFEJOINT addresses this challenge by developing novel techniques for metal to metal and metal to composite joining as well as developing novel techniques for the non-destructive inspection and evaluation of such joints in order to enhance confidence to designers and end-users of hybrid structures of their through life safe performance. SICOMP's role in the project is to develop a design methodology for prefabricated metal to composite joints containing both chemical and mechanical adhesion with the capacity to both predict damage initiation and progression in the joint itself and in the surrounding composite structure. Swerea SICOMP will also, together with Swerea IVF, use carbon nanotubes to strengthen the hybrid joints both in the joint itself and in the surrounding composite material.

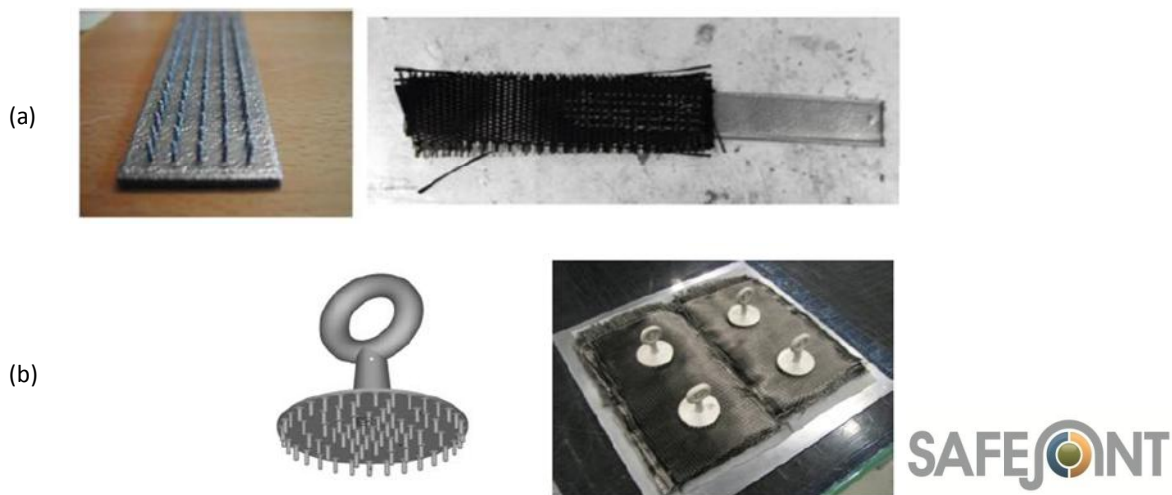


Figure 3.5.3-1. (a) Prefabricated single overlap specimen, (b) peel test specimen.

### 3.5.4 Cryogenic Hypersonic Advanced Tank Technologies (CHATT)

In future aviation and particularly in hypersonic systems new propellants will be used, such as liquid hydrogen, liquid methane and possibly even liquid oxygen. These systems will require complex technology, ultra light-weight and reusable propellant tank systems. New materials and design concepts are required such as polymer based fibre composites in order to reduce the tank weight and to increase the structural performance. In the CHATT project [16], Swerea SICOMP will mainly be involved in the structurally related difficulties associated with CFRP propellant tanks for reusable aerospace vehicles. The aim of this work is to perform, within Europe, an extensive cryogenic CFRP tank investigation, including tank demonstration and development beyond the current state-of-art. The work concerns selection of state-of-the-art materials such as liner and composite materials. Sample tests are performed to support the final goal; the development and testing of scaled tank demonstrators. All advanced cryogenic tank technologies to be investigated within CHATT are driven by system demands of future hypersonic passenger configurations. All cryo-tank technologies should eventually be assessed by the system requirements. These vehicles have already been proposed a few years ago and are under study in the EU-funded cooperative projects LAPCAT and FAST20XX: LAPCAT A2, LAPCAT M8, and the SpaceLiner.

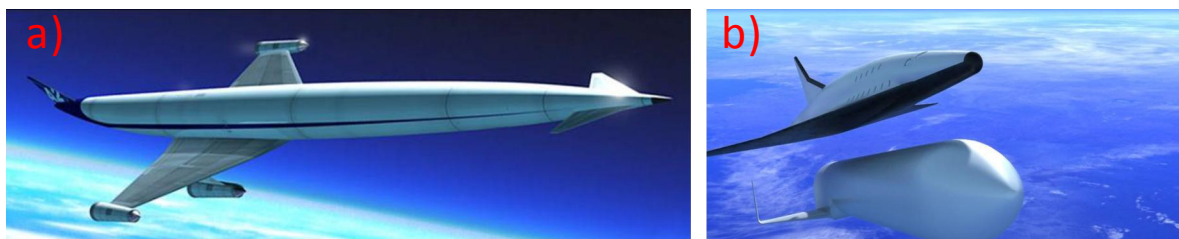


Figure 3.5.4-1: a) LAPCAT A2 hypersonic Mach 5 Civil Transport, b) SpaceLiner hypersonic passenger transport

### 3.6 NDT TECHNOLOGY

#### 3.6.1 Detectability of indents after impact in full-scale CFRP wing skins

Damage tolerance of carbon composite structure is to a large extent conditional on impact damages. In MIL-STD-1530 and JSSG-2006 is the “barely visible impact damage” BVID criterion defined as a damage from an impactor (1.0" diameter hemispherical) with 100 ft-lbs (135.6 J) of kinetic energy or with that kinetic energy required to cause a dent 0.10" (2.54 mm) deep, whichever is less. The indent depth is assumed to be detected by the naked eye under a visual inspection from a distance of 5 ft (1.5 m). Most often is a general criterion defined for a reduced energy level and indent magnitudes due to the assumed overly severe original criterion. The BVID criterion is in typical cases set to damage from an impactor with 50J of kinetic energy or with that kinetic energy required to cause a dent 1 mm deep, whichever is less. Design data e.g. CAI are often based on tests on simple specimens under such assumptions.

After completion of all testing and tear down examinations of the Gripen single seater full scale fatigue test was one of the wings saved for impact tests. The purpose of the test was to obtain experimental information on a real full-scale structure regarding BVID detectability with reduced kinetic energy levels and the reduced indent depth. Conventional impact test equipment was used having a hemispherical impactor with a tip diameter of 25 mm (1 inch). The equipment was moved around to the preselected impact sites and fixed in position by adjustment screws and by placing heavy lead blocks on the bottom frame.

The impact positions were selected to represent different skin thicknesses, layups, thickness step areas and distances to inner structures such as spars and ribs. The obtained damages in terms of indent depth and projected delamination size was measured.

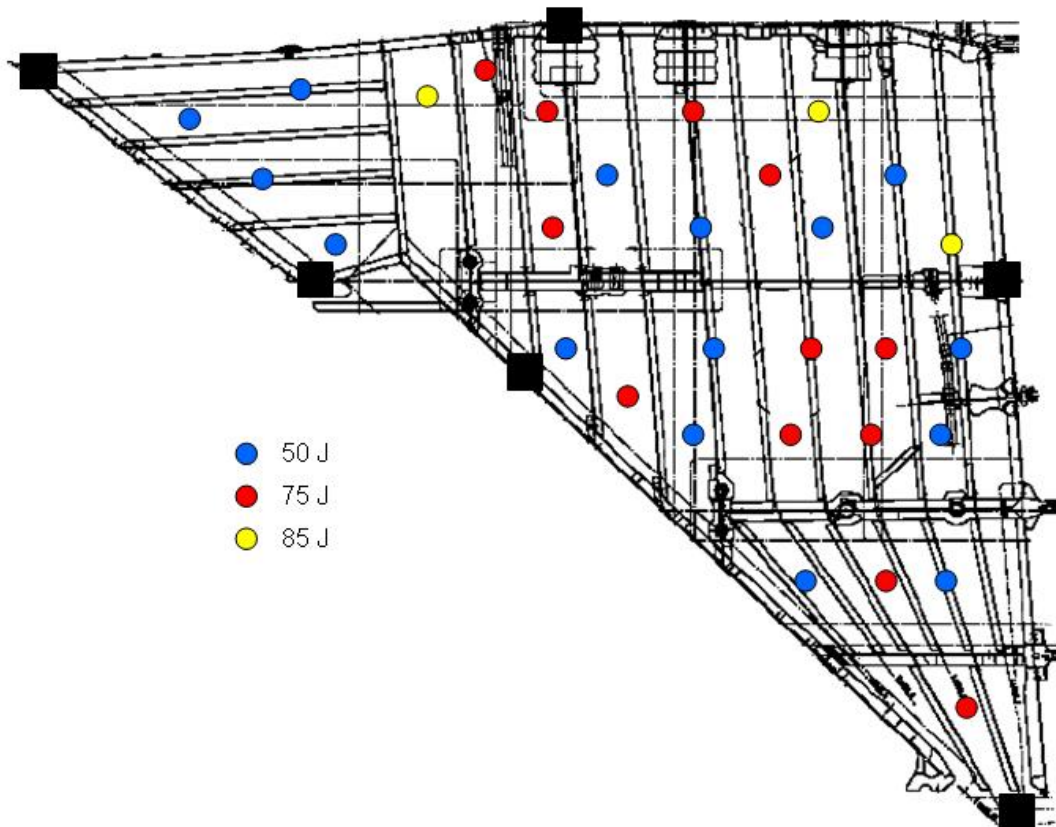


Figure 3.6.1-1. Impact positions and energy levels

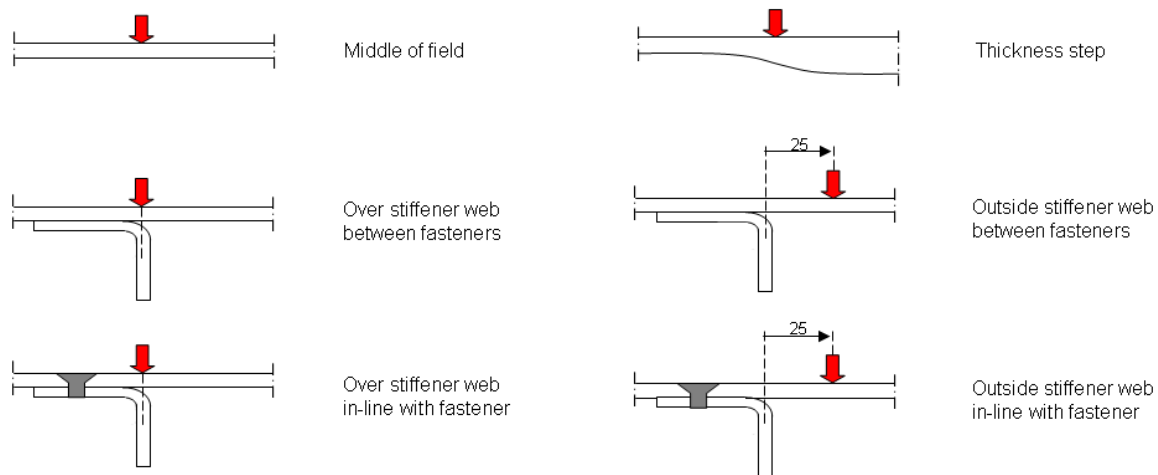


Figure 3.6.1-2. Impact positions regarding proximity to inner structure

All impact areas were measured regarding projected delamination area using ultra sonic techniques and a selected number of damage areas were cut from the wing skin and examined in microscope.

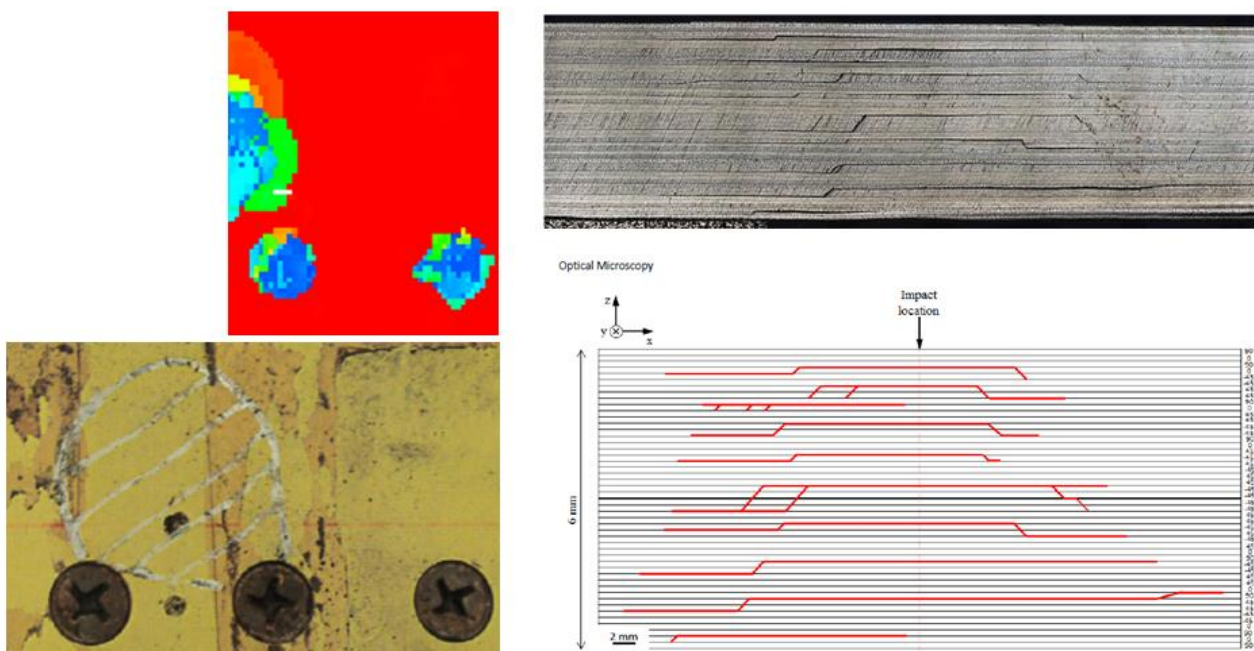


Figure 3.6.1-3. Example of projected impact damage area from ultra sonic measurement and from microscope examination on cut pieces.

The prime aim of the tests was however to measure the indent depth in order to get a picture of the detectability under the BVID criterion on a real structure, i.e. minimum 1 mm indent depth. Not at any of the 30 impact positions was a visible indent observed i.e. the measured indents were less than 1/10 of a millimeter (due to lack of visual indentation during testing, the impact energies were increased above the preselected cut-off energy of 50 J). The conclusion was that the BVID criterion did not meet the detectability requirement and therefore not useful for damage detection even though damages were present.

### 3.7 SERVICE LOADS MONITORING

#### 3.7.1 A flight parametric method for loads and fatigue life monitoring of Gripen C/D aircraft

The Gripen fighter aircraft system has since the A/B versions were introduced been equipped with a strain gauge based loads monitoring system for service life monitoring. Further demands regarding direct links to each life limiting structural part and to data fusion in the ground maintenance system for C/D versions have required a development of the system. The new system is based on flight and configuration parameters and is processed on ground, [17].

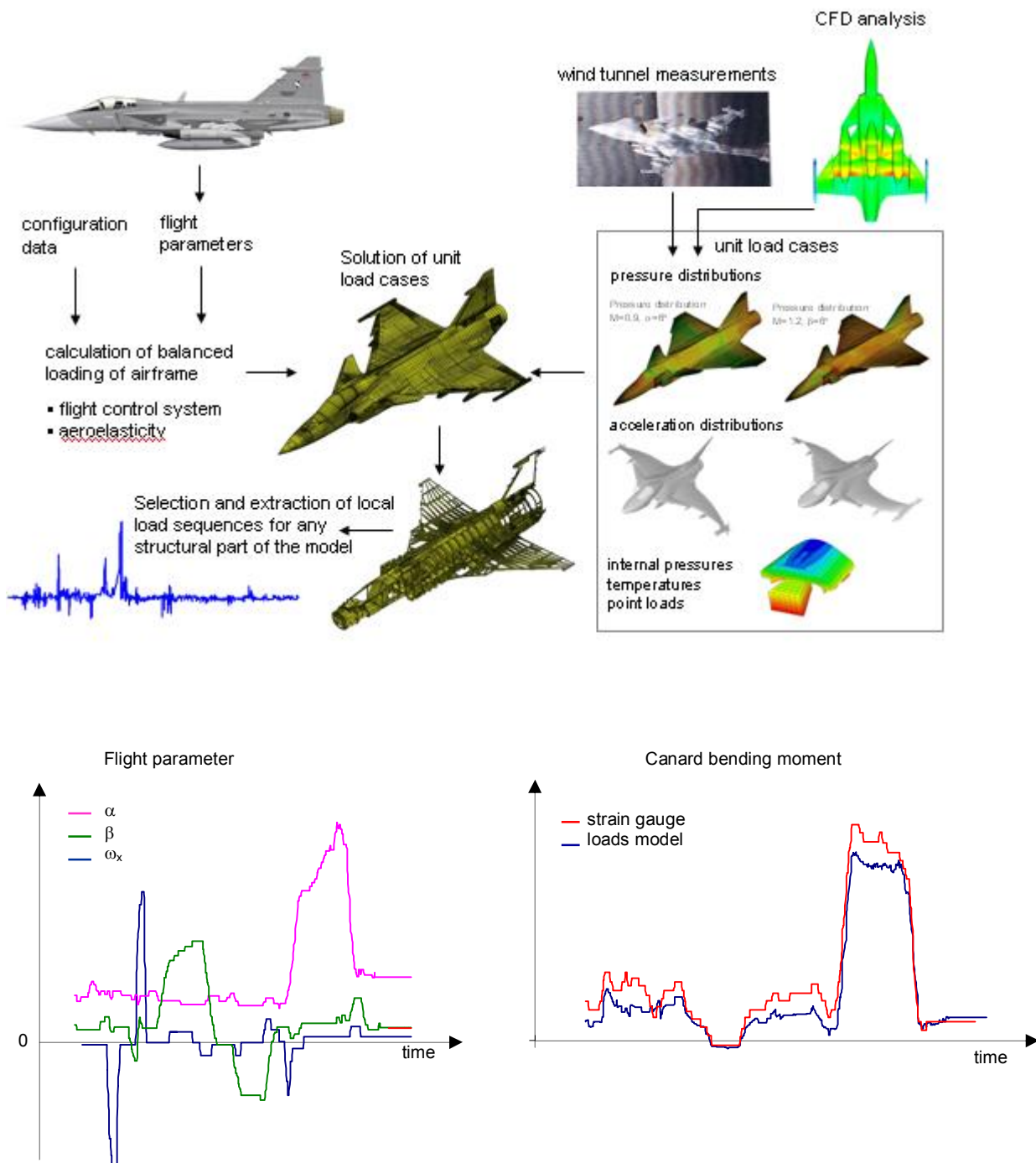
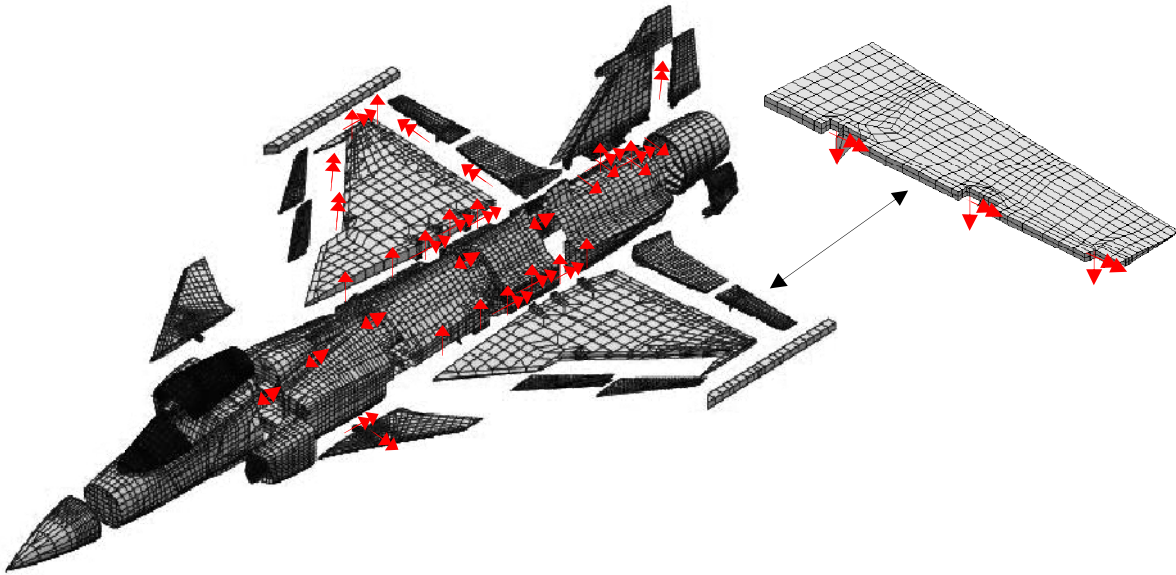


Figure 3.6.2-1. Loads model converting monitored flight parameters to loads sequences

The system covers all flight critical parts and other structural significant parts as well as all weapon pylons and their attachments to the airframe. A total of about 150 principal load entities have been selected for this purpose.



*Figure 3.6.2-2. Examples of monitored load entities of the airframe*

The system enables monitored parts to be replaced and switched between different aircraft. The paper describes the required parameter data and the models, loads and fatigue, used for the instantaneous fatigue life consumption. It also describes an indirect account, through a synthetic event model for dynamic events not fully covered by the system due to insufficient sampling rates e.g. stores release. The efforts of migration of historic flight data to aircraft already in service are outlined as well as some real flight analysis of different types. The system will be inherited into the E/F versions with necessary changes due to structural differences.

## REFERENCES

- [1] ICAF Doc.No 2411. A review of aeronautical fatigue investigations in Sweden during the period June 2005 to April 2007. Edited by Ansell, H. Presented at the 30th Conference of the International Committee on Aeronautical Fatigue (ICAF), Naples, Italy, 14-15 May 2007.
- [2] ICAF Doc.No 2419. A review of aeronautical fatigue investigations in Sweden during the period May 2007 to April 2009. Edited by Ansell, H. Presented at the 31th Conference of the International Committee on Aeronautical Fatigue (ICAF), Rotterdam, The Netherlands, 24-25 May 2009.
- [3] ICAF Doc.No 2426. A review of aeronautical fatigue investigations in Sweden during the period May 2009 to March 2013. Edited by Ansell, H. Presented at the 32<sup>th</sup> Conference of the International Committee on Aeronautical Fatigue (ICAF), Montreal, Canada, 29-31 May 2011.
- [4] Zlatan Kapidzic, Markus Johanson, Thomas Johansson, Urban Wendt, Hans Ansell. Damage Tolerance Test and Analysis of Wing Tip Pylons for the Gripen Aircraft. Presented at the 27<sup>th</sup> Symposium of the International Committee on Aeronautical Fatigue (ICAF), Jerusalem, Israel, 5-7 June 2013.
- [5] Z. Kapidzic, L. Nilsson, H. Ansell, (2013), Conceptual studies of a composite aluminum hybrid wing box demonstrator, Submitted.
- [6] Z. Kapidzic, L. Nilsson, H. Ansell, (2013), Finite element modeling of mechanically fastened composite-aluminum joints in aircraft structures, Submitted.
- [7] Z. Kapidzic, R. Gutkin, (2013), Detailed modeling of low velocity impact on a hybrid wing box structure, Submitted to 4:th CEAS Air & Space Conference, September 16-19, 2013.
- [8] D. Gustafsson, J.J. Moverare, S. Johansson, K. Simonsson, M. Hörnqvist, T. Månsson, S. Sjöström, Influence of high temperature hold times on the fatigue crack propagation in Inconel 718, *International Journal of Fatigue*, 33(11) (2011) 1461-1469.
- [9] P. Heuler, E. Affeldt, R.J.H. Wanhill, Effects of Loading Waveform and Stress Field on High Temperature Fatigue Crack Growth of Alloy 718, *Materialwissenschaft und Werkstofftechnik*, 34(9) (2003) 790-796.
- [10] J.P. Pédrón, A. Pineau, The effect of microstructure and environment on the crack growth behaviour of Inconel 718 alloy at 650°C under fatigue, creep and combined loading, *Materials Science and Engineering*, 56(2) (1982) 143-156.
- [11] U. Krupp, Dynamic embrittlement - time-dependent quasi-brittle intergranular fracture at high temperatures, *International Materials Reviews*, 50 (2005) 83-97.
- [12] Holmberg, E.: Stress and fatigue constrained topology optimization. Linköping Studies in Science and Technology, Licentiate Thesis No. 1571. ISBN 978-91-7519-703-6. 2013. <http://urn.kb.se/resolve?urn=urn:nbn:se:liu:diva-88094>
- [13] Holmberg, E., Torstenfelt, B., Klarbring, A.: Stress constrained topology optimization. *Structural and Multidisciplinary Optimization*. DOI 10.1007/s00158-012-0880-7. 2012
- [14] Holmberg, E., Torstenfelt, B., Klarbring, A.: Fatigue constrained topology optimization. Submitted for publication. 2013

- [15] Henriksson, K: An experimental study of rotation in a composite single bolted joint. Master-thesis, Uppsala University, 2012. <http://urn.kb.se/resolve?urn=urn:nbn:se:uu:diva-176844>
- [16] Grant agreement for: Collaborative project, Annex I - "Description of Work", Project acronym: CHATT, Project full title: "Cryogenic Hypersonic Advanced Tank Technologies", Grant agreement no: 285117, Version date: 2011-07-11, PART B
- [17] Hans Ansell, Thomas Johansson. A flight parametric method for loads and fatigue life Monitoring of Gripen C/D aircraft. Presented at the 27<sup>th</sup> Symposium of the International Committee on Aeronautical Fatigue (ICAF), Jerusalem, Israel, 5-7 June 2013.

## ACKNOWLEDGEMENTS

This work was supported by Saab AB. The editor is also indebted to the following individuals who helped to write this review:

David Gustafsson	LiU	(Section: 3.4.2)
Renaud Gutkin	Swerea SICOMP	(Section: 3.3.7)
Karolin Henriksson	FOI	(Section: 5.5.2)
Erik Holmberg	SAAB AB	(Section: 3.4.3)
Markus Johansson	SAAB AB	(Section: 3.3.6)
Thomas Johansson	SAAB AB	(Section: 3.3.6, 3.7.1)
Zlatan Kapidzic	SAAB AB	(Section: 3.3.6, 3.3.7, 3.4.1, 3.5.1)
Carolina Lara Silva	SAAB AB	(Section: 3.4.1)
Robin Olsson	Swerea SICOMP	(Section: 3.5.3, 3.5.4)
Joakim Schön	FOI	(Section: 3.3.7, 3.5.1, 3.5.2)
Stefan Thuresson	SAAB AB	(Section: 3.2.1, 3.2.2, 3.3.1, 3.3.2)
Urban Wendt	SAAB AB	(Section: 3.3.6)